nature communications

Article

https://doi.org/10.1038/s41467-024-55609-9

Noradrenergic inputs from the locus coeruleus to anterior piriform cortex and the olfactory bulb modulate olfactory outputs

Received: 27 July 2023

Accepted: 17 December 2024

Published online: 02 January 2025

Check for updates

Chi Geng[1,5], Ruochen Li[1,5], Shan Li[1,5], Penglai Liu[1], Yuxin Peng[1], Changyu Liu[1], Zhen Wang[1], Hongxing Zhang[2,3,4] & Anan Li[1]

Norepinephrine (NE) released from locus coeruleus (LC) noradrenergic (NAergic) neurons plays a pivotal role in the regulation of olfactory behaviors. However, the precise circuits and receptor mechanisms underlying this function are not well understood. Here, in DBH-Cre mice model, we show that LC NAergic neurons project directly to both anterior piriform cortex (aPC) and the olfactory bulb (OB). By using pharmacological and optogenetic manipulations in vitro and in vivo, we found that NE reduces the excitability of aPC pyramidal neurons directly via α2 receptors and that it bidirectionally regulates the activity of OB mitral cells via modulation of inhibitory inputs. Activation of the NAergic projection reduced both spontaneous and odor-evoked activity in the aPC/OB in awake mice, enhanced the odor-decoding ability of the aPC, and decreased the odor-decoding ability of the OB. Furthermore, activation of LC–aPC/OB NAergic projections accelerated odor discrimination and specific inactivation of the LC–aPC/OB NAergic pathway impaired olfactory detection and discrimination. These findings identify the mechanism underlying NAergic modulation of the aPC/OB and elucidate its role in odor processing and olfactory behaviors.

The olfactory bulb (OB) is the first information processing center in the olfactory system. It receives neural signals directly from the olfactory sensory neurons, where the olfactory receptors are located. Mitral/tufted cells (M/Ts) are output neurons that send the processed information from the OB to the olfactory cortex via the lateral olfactory tract[1–3]. One direct target of the M/T projection is the anterior piriform cortex (aPC), which is one of the most important olfactory cortices[1,4,5]. Functionally, the OB and aPC are critically involved in the neural representation of odor identity, odor concentration, and odor value[2,6–10]. As well as unique neural circuits within the OB and aPC, regulation by modulatory systems also contributes to these functions, including serotonergic modulation from the dorsal raphe nucleus[11–13], cholinergic modulation from the horizontal limb of the diagonal band of Broca[14–17], and noradrenergic (NAergic) modulation from the locus coeruleus (LC)[18–21].

The LC is located within the brain stem. It sends extensive projections throughout the brain and predominantly releases noradrenaline (NE) and other types of neurotransmitters to modulate arousal, attention, and memory[18,19,22–24]. Although less studied, NE also plays an essential role in regulating olfaction[25–29]. The OB and aPC both receive extensive centrifugal inputs from LC NAergic neurons[21,30,31] and three adrenergic receptors (α1, α2, and β) are expressed in the aPC and OB[32–34], suggesting potential NAergic modulation of the aPC and OB. Several studies have investigated how LC noradrenergic inputs

[1]Jiangsu Key Laboratory of Brain Disease and Bioinformation, Research Center for Biochemistry and Molecular Biology, Xuzhou Medical University, Xuzhou, Jiangsu, China. [2]Jiangsu Province Key Laboratory of Anesthesiology, Xuzhou Medical University, Xuzhou, Jiangsu, China. [3]Jiangsu Province Key Laboratory of Anesthesia and Analgesia Application Technology, Xuzhou Medical University, Xuzhou, Jiangsu, China. [4]NMPA Key Laboratory for Research and Evaluation of Narcotic and Psychotropic Drugs, Xuzhou Medical University, Xuzhou, Jiangsu, China. [5]These authors contributed equally: Chi Geng, Ruochen Li, Shan Li. e-mail: anan.li@xzhmu.edu.cn

modulate neural activity in the OB and aPC. For example, electrical stimulation of the LC modulates spontaneous and odor-evoked neural activity of the aPC/OB in animals under anesthesia[35,36]. Pharmacological studies have shown that NE regulates the synaptic transmission of aPC pyramidal neurons and mitral cells in a concentration-dependent manner[33,37,38]. Behaviorally, while bulbar infusion of α1 receptor antagonists suppresses odor discrimination and blockade of OB β receptors improves odor discrimination[39,40], blockade of β receptors in piriform cortex weakens odor preference learning[37]. These studies suggest that the effects of NE on olfaction are region or circuit specific. Although these previous studies attempted to delineate the mechanism and function of NE regulation of the aPC and OB, direct evidence indicating how LC NAergic neurons modulate olfaction via the aPC/OB is still lacking, and whether these three brain regions collaborate to modulate olfaction remains elusive.

In this study, we identified the olfactory circuits connecting the aPC/OB and LC and the mechanism by which NE regulates activity in the aPC/OB. We also investigated how NAergic neurons modulate the odor-evoked responses and odor-decoding ability of aPC pyramidal neurons and OB mitral cells in awake mice and further elucidated the role of the LC–aPC/OB pathway in the regulation of olfactory behaviors.

Results

LC NAergic neurons project directly to both the aPC and the OB

Previous studies have reported that the LC projects to olfactory areas. Data derived from tracer mapping and viral labeling experiments suggest that both the aPC and OB receive inputs from the LC[20,21,30,31]. To further investigate the anatomical connections and identity of aPC-projecting and OB-projecting LC neurons, we used anterograde and retrograde labeling to characterize the projections.

First, the LC–aPC and LC–OB projections were studied with anterograde labeling. We injected a Cre-dependent virus encoding yellow fluorescent protein, AAV-DIO-eYFP, into the LC of DBH-Cre mice to selectively infect NAergic neurons (Fig. 1A). After 4 weeks, eYFP-expressing neurons were observed in the LC, and ~95% of these neurons were immunoreactive for TH (Fig. 1B–D). Dense projection fibers co-labeled with TH were observed in the aPC and OB (Fig. 1E, F). These results show that LC NAergic neurons send direct projections to the aPC and OB.

Next, retrograde labeling was used to verify the LC–aPC and LC–OB projections. We retrogradely labeled aPC-projecting LC neurons and OB-projecting LC neurons by injecting a Cre-dependent retrograde transport virus, AAV-retro-DIO-eYFP, into the aPC (Fig. 1G) or OB (Fig. 1J) of DBH-Cre mice. eYFP-expressing neurons co-labeled with TH were found in the LC (Fig. 1H, I, K, L). These results provide further evidence that LC NAergic neurons project directly to the aPC and OB.

Previous studies have shown that individual LC NAergic neurons can innervate multiple brain regions that are far apart from each other[41]. We postulated that individual LC NAergic neurons that project to the aPC could also project to the OB. To test this hypothesis, we used dual-retrograde labeling: we injected AAV-retro-DIO-eYFP into the OB and AAV-retro-DIO-mCherry into the aPC of DBH-Cre mice to label OB-projecting LC neurons and aPC-projecting LC neurons, respectively (Fig. 1M). We found that 84.38 ± 2.86% of eYFP-expressing cells and 89.19 ± 1.75% of mCherry cells in the LC were co-labeled with TH (Fig. 1N–P). This colocalization rate is relatively high and is comparable to another study[22]. We further analyzed the proportion of NAergic neurons projecting to the aPC and OB and found that 11.81 ± 1.02% (on average 7.36 ± 0.63 from 65.61 ± 4.04 cells, n = 28 sections) LC NAergic neurons projected to the OB, 24.82 ± 1.59% (on average 15.18 ± 0.83 from 65.61 ± 4.04 cells, n = 28 sections) projected to the aPC, and 9.04 ± 0.79% (on average 5.54 ± 0.45 from 65.61 ± 4.04 cells, n = 28 sections) projected to both the aPC and OB (Fig. 1Q–S). Furthermore, 77.79 ± 2.92% of the OB-projecting LC eYFP$^+$/TH$^+$ neurons were co-labeled with mCherry, indicating that a large proportion of OB-projecting LC NAergic neurons also project to the aPC (Fig. 1T). However, only 37.84 ± 3.08% of aPC-projecting LC mCherry$^+$/TH$^+$ neurons were co-labeled as OB-projecting eYFP$^+$ neurons (Fig. 1U). These results suggest that there are two main types of LC NAergic neurons that project to the aPC and the OB: one type projects to both the aPC and the OB (type I), and the other type projects only to the aPC (type II).

Moreover, to provide images of the full axonal projection from LC NAergic neurons to the aPC and OB, we selectively labeled a small number of NAergic neurons by injecting the Cre-dependent virus AAV-sparse-CSSP-eYFP-2E4 into the LC of DBH-Cre mice. After 4 weeks, the eYFP-expressing NAergic neurons were observed in the LC and the full extent of the projection fibers to the OB and aPC were captured by 3-D tissue imaging (Supplementary Fig. 1A–D and Supplementary Movie 1). This result provides the direct evidences of the two main types of the LC NAergic neurons project to the aPC and OB.

To explore whether there are potential functional differences between these two main types of LC NAergic neurons, we analyzed their electrophysiological characteristics via whole-cell recordings. The frequency of current-evoked action potentials (APs) (Supplementary Fig. 2A, B), the frequency of spontaneous APs in cell-attached mode (Supplementary Fig. 2C, D), the frequency of spontaneous APs in current-clamp mode (Supplementary Fig. 2E, F), the input resistance (Supplementary Fig. 2G), and the resting membrane potential (RMP) (Supplementary Fig. 2H) were not significantly different between the two groups. These results indicate that there are no differences in the electrophysiological properties of these two types of NAergic neurons.

NE decreases the excitability of aPC pyramidal neurons via α2 receptors

The morphological results described above suggest that NE may regulate activity in the aPC/OB. To investigate whether LC NAergic neurons make functional synaptic connections with aPC pyramidal neurons, we first performed whole-cell recordings in aPC pyramidal neurons to examine the modulatory effects of NE. We recorded current-evoked APs from aPC layer 2/3 pyramidal cells in slices from adult mice in response to different intensities of current injection (Fig. 2A). The frequency of APs increased with the size of the current step. Bath application of NE (10 μM) significantly reduced the frequency of APs (Fig. 2B, C). In addition, NE hyperpolarized the RMP of aPC pyramidal neurons (Fig. 2D) but had no effect on AP threshold (Fig. 2E). To further study the effect of NE on the neural activity of aPC pyramidal neurons, we recorded spontaneous inhibitory postsynaptic currents (sIPSCs) and spontaneous excitatory postsynaptic currents (sEPSCs) from aPC pyramidal neurons in slices from adult mice. NE (10 μM) increased the amplitude, but not the frequency, of sIPSCs (Fig. 2F, G), Neither the amplitude nor the frequency of sEPSCs was altered by application of NE (Fig. 2H, I). These results indicate that NE decreases the excitability of aPC pyramidal neurons.

It is well established that all three types of adrenoceptors (α1, α2, and β) are expressed in the aPC[34]. We therefore performed experiments to investigate which adrenoceptors mediate the inhibitory effect of NE. Current-evoked APs were recorded in the presence of yohimbine (2 μM), an α2 receptor blocker. NE (10 μM) failed to decrease the frequency of APs or hyperpolarize the RMP of aPC pyramidal neurons in the presence of yohimbine (Fig. 2J). However, the α1 receptor antagonist prazosin and the β receptor antagonist propranolol had no effect on NE-induced inhibition (Fig. 2K, L). These results show that the inhibitory effect of NE on aPC pyramidal neurons is mediated by α2 receptors.

Together, these results demonstrate that NE decreases the excitability of aPC pyramidal neurons via α2 receptors.

https://doi.org/10.1038/s41467-024-55609-9

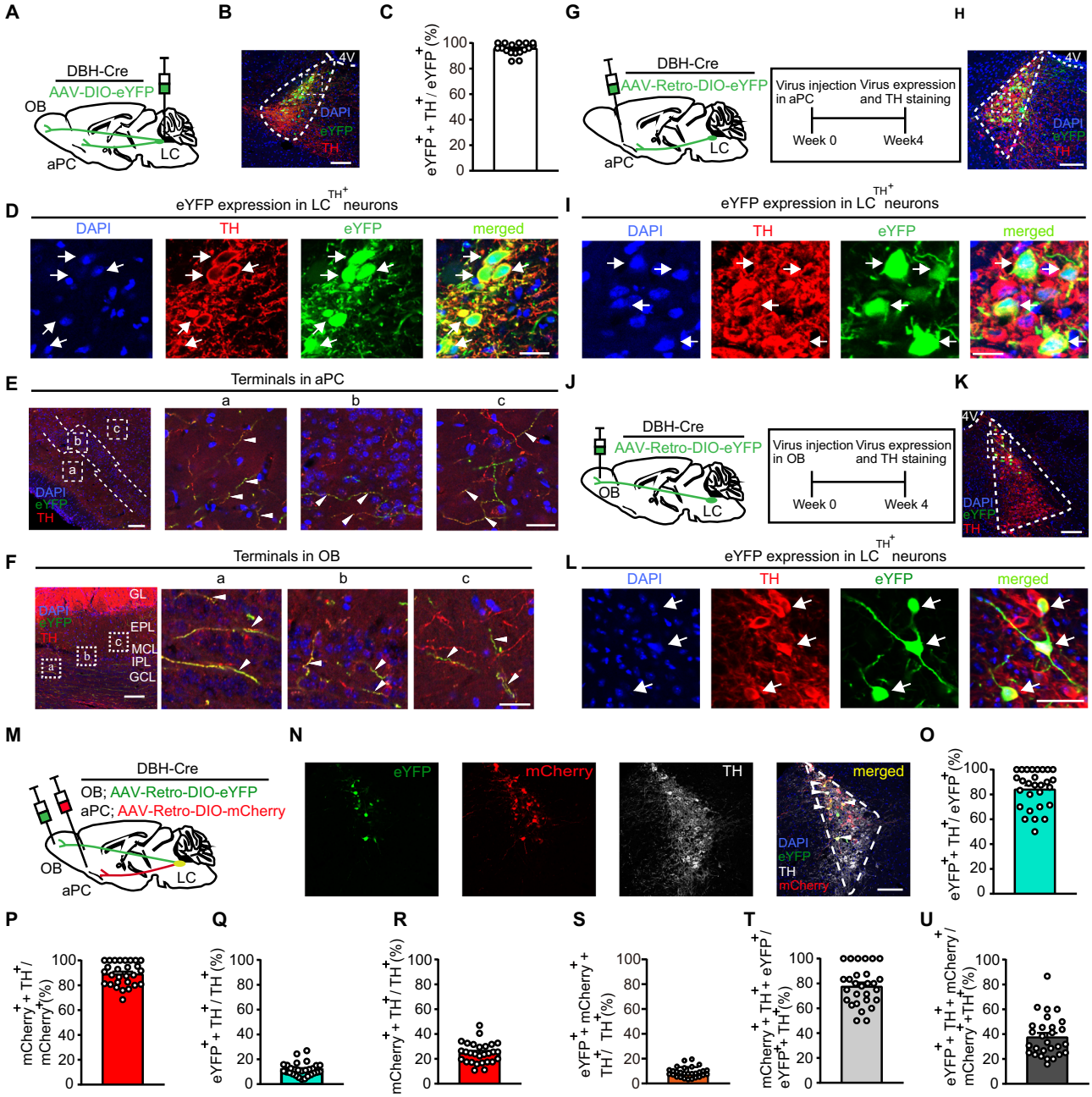

Fig. 1 | LC NAergic neurons project directly to both the aPC and the OB. **A** Schematic of the anterograde LC–aPC/OB projection-labeling strategy. **B** Immunohistochemistry (IHC) showing co-labeling of TH staining with eYFP-labeled neurons in the LC (blue, DAPI; green, eYFP; red, TH; scale bar, 100 μm). **C** Percentage of eYFP$^+$ neurons in the LC that were immunoreactive for TH (n = 17 sections from 4 mice). **D** Enlarged area from B (arrows indicate examples of colocalization; scale bar, 25 μm). IHC showing co-labeling of TH staining with eYFP$^+$ fibers from LC eYFP$^+$ neurons in the aPC (**E**) and in the OB (**F**) (blue, DAPI; green, eYFP; red, TH; arrows, co-localization examples; scale bars: left, 100 μm; right, 25 μm). **G** Schematic of the retrograde tracing of the LC–aPC circuit and the experimental timeline. Co-labeling of TH staining with eYFP$^+$ neurons in the LC (**H**; blue, DAPI; green, eYFP; red, TH; scale bar, 100 μm) and enlarged areas from (**H**) (**I**; scale bar, 20 μm). **J** Schematic of the retrograde tracing of the LC–OB circuit and experimental timeline. Co-labeling of TH staining with eYFP$^+$ neurons in the LC (**K**; blue, DAPI; green, eYFP; red, TH; scale bar, 100 μm) and enlarged areas from (**K**) (**L**; scale bar, 50 μm). Schematic of the dual retrograde tracing of the LC–aPC/OB pathways (**M**) and co-labeling of TH staining with eYFP$^+$ neurons and mCherry$^+$ neurons in the LC (**N**; blue, DAPI; green, eYFP; red, mCherry; white, TH; scale bar, 100 μm). Percentage of LC eYFP$^+$ neurons (**O**) or mCherry$^+$ neurons (**P**) immunoreactive for TH. n = 28 sections from 3 mice. Percentage of NAergic neurons projecting to the OB (**Q**), the aPC (**R**), and both the OB and aPC (**S**). n = 28 sections from 3 mice. **T** Percentage of mCherry$^+$/TH$^+$/eYFP$^+$ colocalization in all eYFP$^+$/TH$^+$ neurons. **U** Percentage of eYFP$^+$/TH$^+$/mCherry$^+$ colocalization in mCherry$^+$/TH$^+$ neurons. n = 28 sections from 3 mice. 3 independent repetitions with similar results in (**E**, **F**, **H**, **I**, **K**, **L**). Data are presented as the means ± SEM.

Optogenetic stimulation of LC–aPC NAergic terminals decreases the activity of aPC pyramidal neurons via α2 receptors

Our in vitro pharmacological experiments demonstrated the modulatory effect of NE on aPC pyramidal neurons and identified the underlying mechanism. We next confirmed the effect of NE on aPC pyramidal neurons by specific activation of the LC–aPC NAergic terminals. To achieve this, we injected a Cre-dependent virus encoding channelrhodopsin-2 (AAV-DIO-ChR2-eYFP) into the LC of DBH-Cre mice to enable selective activation of the LC–aPC NAergic terminals by illumination with 473-nm blue light (Fig. 3A and Supplementary

https://doi.org/10.1038/s41467-024-55609-9

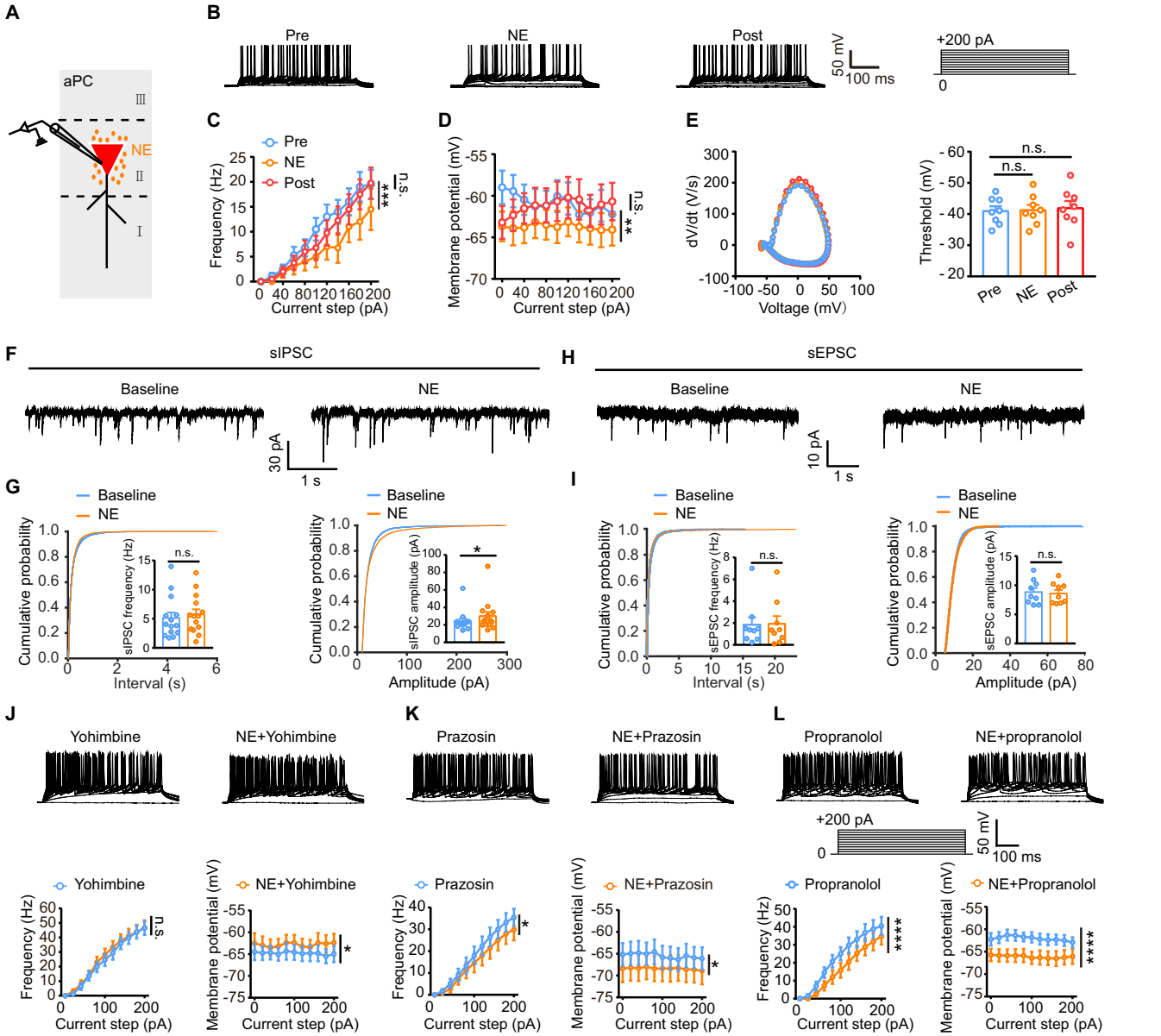

Fig. 2 | NE decreases the activity of aPC pyramidal neurons via α2 receptors. **A** Schematic of whole-cell recordings. **B** Sample traces showing action potentials (APs) before, during, and after application of NE. Quantitative analysis of the frequency of current-evoked APs (**C**; Pre versus NE, $p = 0.00030$, $q = 5.62$; Post versus Pre, $p = 0.35$, $q = 1.95$; two-way ANOVA, $n = 10$ cells from 5 mice), membrane potential (**D**; Pre versus NE, $p = 0.0024$, $q = 4.77$; Post versus Pre, $p = 0.87$, $q = 0.72$, two-way ANOVA, $n = 10$ cells from 5 mice), and threshold (**E**; Pre versus NE, $p = 0.99$, $q = 0.11$; Post versus Pre, $p = 0.92$, $q = 0.34$; one-way ANOVA, $n = 8$ from 5 mice) before, during, and after bath application of NE. **F**–**I** Representative sIPSC (**F**) and sEPSC (**H**) traces from aPC pyramidal neurons before and during application of NE. Quantitative analysis of the frequency and amplitude of sIPSCs (frequency, $p = 0.47$, $z = -0.72$; amplitude, $p = 0.048$, $z = -1.98$; two-tailed Wilcoxon matched-pairs signed rank test; $n = 14$ cells from 5 mice; **G**) and sEPSC (frequency, $p = 0.86$, $z = -0.18$, two-tailed Wilcoxon matched-pairs signed rank test; amplitude, $p = 0.55$, $t_{(8)} = 0.63$, two-sided paired t-test; $n = 9$ cells from 4 mice; **I**) upon NE treatment. **J**–**L** Yohimbine, but not prazosin or propranolol, blocked the decreased AP frequency and reduction in membrane potential induced by NE. **J** Frequency, $p = 0.33$, $F_{(1,\ 242)} = 0.93$; membrane potential, $p = 0.013$, $F_{(1,\ 242)} = 6.20$, two-way ANOVA, $n = 12$ cells from 5 mice; (**K**) frequency, $p = 0.039$, $F_{(1,\ 308)} = 4.29$; membrane potential, $p = 0.015$, $F_{(1,\ 308)} = 5.96$, two-way ANOVA, $n = 15$ cells from 6 mice; (**L**) frequency, $p < 0.0001$, $F_{(1,\ 198)} = 15.84$; membrane potential, $p < 0.0001$, $F_{(1,\ 198)} = 49.11$, two-way ANOVA, $n = 10$ cells from 3 mice. Data are presented as the means ± SEM. *$p < 0.05$, **$p < 0.01$, ***$p < 0.001$, ****$p < 0.0001$. ns no significance.

Fig. 3A). After allowing four weeks after injection for viral expression, ChR2-eYFP$^+$ neurons were identified in the LC (Supplementary Fig. 3B) and ChR2-eYFP$^+$ terminals were observed in the aPC (Fig. 3B). In LC NAergic ChR2-eYFP$^+$ neurons, light evoked rapid inward currents (Supplementary Fig. 3C, D). Furthermore, light delivered for at 5 Hz, 10 Hz, and 20 Hz lights for 1 min reliably evoked a continuous train of inward currents, indicating that all three frequencies of light delivery were effective for activating LC NAergic neurons (Supplementary Fig. 3E). Next, to test whether activation of LC–aPC NAergic terminals regulates the activity of aPC pyramidal neurons, we recorded postsynaptic currents from layer 2/3 pyramidal neurons in the aPC. Optogenetic activation of NAergic terminals (10-ms light pulses at 1 Hz) did not evoke inward currents or outward currents (Fig. 3C). Therefore, this indicates that LC NAergic neurons do not co-release glutamate or GABA to regulate the activity of aPC pyramidal neurons.

To further explore the effect of optogenetic activation of NAergic terminals on the excitability of aPC pyramidal neurons, we recorded the spontaneous firing of aPC layer 2/3 pyramidal neurons in current-clamp configuration. We observed three distinct types of responses to optostimulation (10-ms light pulses at 5 Hz, 10 Hz or 20 Hz for 1 min): 35.71%

https://doi.org/10.1038/s41467-024-55609-9

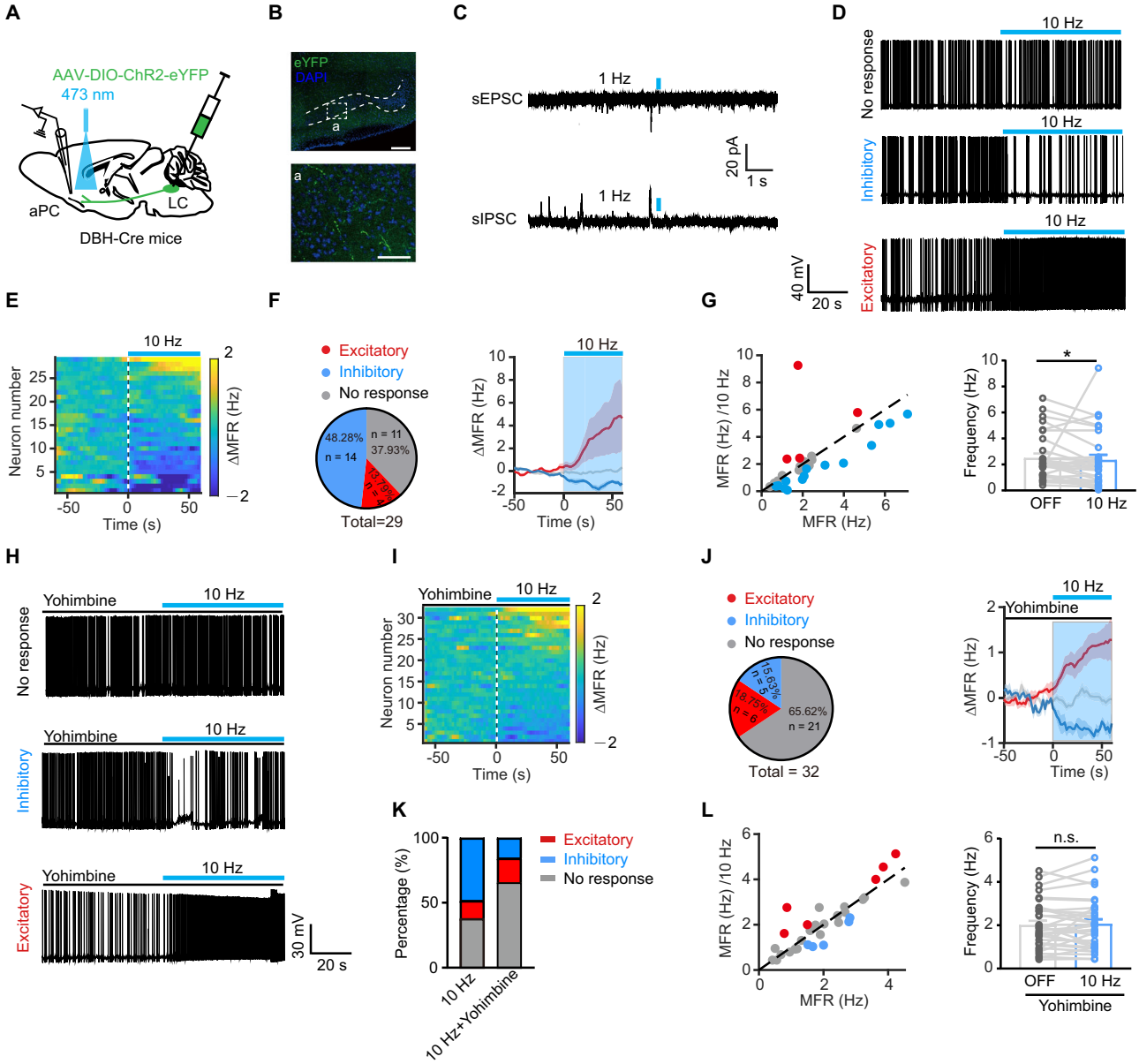

Fig. 3 | Optostimulation of LC–aPC NAergic terminals inhibits the activity of aPC pyramidal neurons via α2 receptors. A Schematic of virus injection and whole-cell recording. **B** The distribution of ChR2-eYFP⁺ NAergic terminals in the aPC (scale bar, 200 μm) and magnification of the indicated region (scale bar, 50 μm). 3 independent repetitions with similar results in (**B**). **C** Representative sEPSC and sIPSC traces recorded from aPC pyramidal neurons with optostimulation (light pulses at 1 Hz, indicated in blue). **D** Raw traces showing three types of responses evoked by optostimulation: excitatory, inhibitory, and no response. Blue lines represent the laser stimulation period. **E** Heat map of all cells ranked by ΔMFR (n = 29 cells from 7 mice). Each row represents one neuron. The dashed line indicates laser onset. **F** The percentages of three types of responses and ΔMFR for all neurons with an excitatory response (red), an inhibitory response (blue), or no response (gray). **G** Comparison of the frequency of spontaneous firing before and during optostimulation ($p = 0.025$, $z = 2.23$, two-tailed Wilcoxon matched-pairs signed rank test). Red, excitatory response; blue, inhibitory response; gray, no response. n = 29 cells from 7 mice. **H** Raw traces showing the three types of responses evoked by optostimulation in the presence of yohimbine (excitatory, inhibitory, and no response). The black line indicates the application of yohimbine and the blue line indicates optostimulation. **I** Heat map of all cells ranked by ΔMFR. Each row represents one neuron (n = 32 cells from 6 mice). **J** The percentages of the three types of responses and ΔMFR for neurons with an excitatory response (red), an inhibitory response (blue), or no response (gray). **K** Distribution of excitatory and inhibitory responses (10 Hz, n = 29 from 7 mice; 10 Hz + yohimbine, n = 32 from 6 mice). **L** Comparison of the frequency of spontaneous firing before and during optostimulation in the presence of yohimbine ($p = 0.58$, $t_{(31)} = 0.56$, two-sided paired t-test, n = 32 cells from 6 mice). Data are presented as the means ± SEM. *$p < 0.05$, ns no significance.

(5 Hz); 48.28% (10 Hz) and 52.38% (20 Hz) of neurons showed decreased firing, 46.43% (5 Hz), 37.93% (10 Hz) and 28.57% (20 Hz) of neurons showed no response, but only 17.86% (5 Hz), 13.79% (10 Hz) and 19.05% (20 Hz) of neurons showed increased firing (Fig. 3D–F and Supplementary Fig. 4A, B, D, E). Of the responsive neurons, 66.67% (5 Hz), 77.78% (10 Hz) and 73.33% (20 Hz) had decreased firing, whereas only 33.33% (5 Hz), 22.22% (10 Hz) and 26.67% (20 Hz) had increased firing. Overall, despite the presence of a few cells with increased firing, activation of LC–aPC NAergic terminals at 10 Hz or 20 Hz, but not 5 Hz, significantly decreased the frequency of APs in aPC pyramidal neurons (Fig. 3G, Supplementary Fig. 4C, F). We also recorded sIPSCs and sEPSCs in aPC pyramidal neurons during optogenetic activation of LC–aPC NAergic terminals. Similar to the bath application of NE described above, optostimulation (10-ms light pulses at 20 Hz for 1 min) of the LC–aPC NAergic terminals increased the amplitude, but not the frequency, of sIPSCs (Supplementary Fig 4G, H). Neither the amplitude nor the frequency of

https://doi.org/10.1038/s41467-024-55609-9

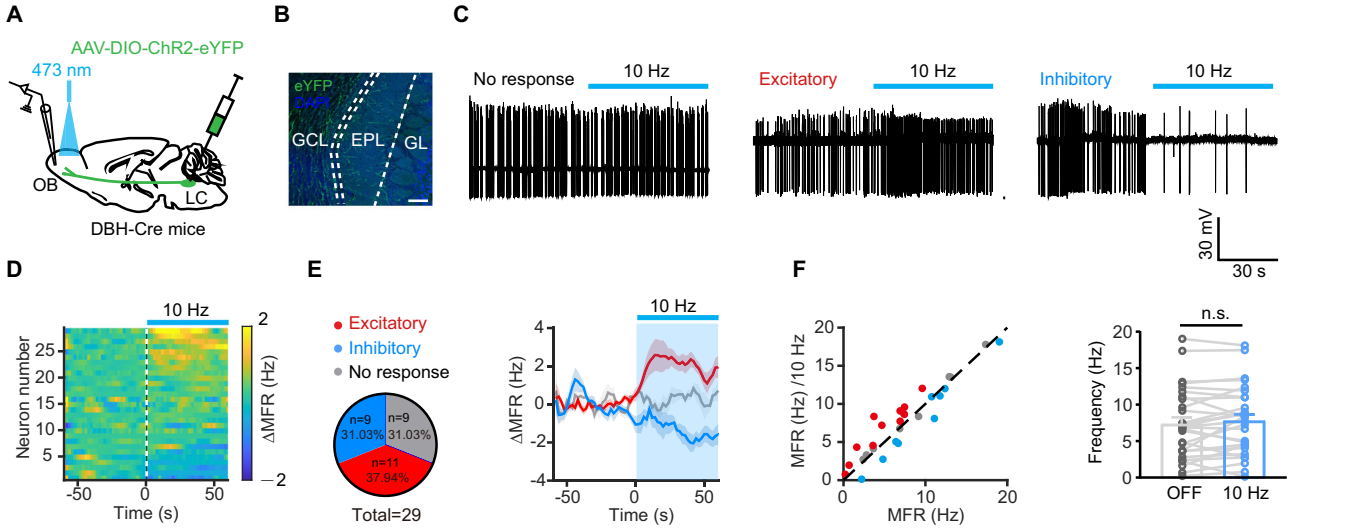

Fig. 4 | Optostimulation of LC–OB NAergic terminals bidirectionally modulates the activity of mitral cells. A Schematic of virus injection and whole-cell recording of mitral cells. **B** The distribution of ChR2-eYFP$^+$ terminals in the OB (scale bar, 100 μm). 3 independent repetitions with similar results in (**B**). **C** Raw traces showing three types of responses evoked by optostimulation: excitatory, inhibitory, and no response. The blue line indicates the laser stimulation period. **D** Heat map of all cells ranked by ΔMFR (n = 29 cells from 8 mice). Each row represents one neuron. The blue line indicates the laser stimulation period and the dashed line indicates laser onset. **E** The percentages of the three types of response and ΔMFR for neurons with an excitatory response (red), an inhibitory response (blue), or no response (gray). The blue line indicates the laser stimulation period. **F** Comparison of the frequency of spontaneous firing before and during optostimulation ($p = 0.18$, $t_{(28)} = 1.37$, two-sided paired t-test, n = 29 cells from 8 mice). Data are presented as the means ± SEM. ns no significance.

sEPSCs was altered by optostimulation (Supplementary Fig 4I, J). These results demonstrate that optogenetic activation of NAergic terminals predominantly inhibits the excitability of aPC pyramidal neurons.

Since the optogenetic results were consistent with the pharmacological findings, we postulated that the inhibitory effect induced by optostimulation may also be mediated by α2 receptors. To test this, we optogenetically activated aPC NAergic terminals (10-ms light pulses at 10 Hz or 20 Hz for 1 min) and recorded the spontaneous firing of aPC pyramidal neurons in the presence of yohimbine. We again observed three types of responses to optostimulation: no response, increased firing rate, and decreased firing rate (Fig. 3H and Supplementary Fig 4K). We analyzed the ratio of these three types of responses across all recorded neurons and found that only 15.63% (10 Hz) or 10% (20 Hz) of neurons showed decreased firing, 18.75% (10 Hz) or 15% (20 Hz) showed increased firing, and a significant proportion of neurons (65.62% for 10 Hz; 75% for 20 Hz) showed no response (Fig. 3I, J and Supplementary Fig 4L, M). The percentage of inhibitory responses induced by optostimulation was significantly decreased in the presence of yohimbine (Fig. 3K and Supplementary Fig 4N). As expected, when we analyzed the population as a whole, optogenetic activation of LC–aPC NAergic terminals did not change the overall frequency of spontaneous firing in the presence of yohimbine (Fig. 3L and Supplementary Fig 4O). These results show that activation of NAergic terminals inhibits the activity of aPC pyramidal neurons through activation of α2 receptors.

Taken together, these optogenetic results and our pharmacological findings consistently indicate that both exogenous NE and NE released from aPC NAergic terminals activate Gi-coupled α2 receptors, ultimately decreasing the excitability of aPC pyramidal neurons.

Activation of LC–OB NAergic terminals bidirectionally regulates the activity of mitral cells by modulating inhibitory transmission

To test the functional contribution of the LC–OB NAergic projection, AAV-DIO-ChR2-eYFP virus was injected into the LC of DBH-Cre mice (Fig. 4A and Supplementary Fig. 5A). ChR2-eYFP$^+$ terminals were observed in the OB (Fig. 4B). We optogenetically activated LC–OB NAergic terminals and recorded the spontaneous firing of mitral cells in cell-attached mode. Three distinct types of responses to optostimulation (10-ms light pulses at 10 Hz or 20 Hz for 1 min) were observed: no response, inhibitory responses, and excitatory responses (Fig. 4C, D and Supplementary Fig 5B, C). Of the recorded neurons, 31.03% (10 Hz) and 46.67% (20 Hz) showed no response, 37.94% (10 Hz) and 23.33% (20 Hz) showed increased firing, and 31.03% (10 Hz) and 30% (20 Hz) showed decreased firing (Fig. 4E and Supplementary Fig 5D). Of the responsive neurons, 45% (10 Hz) and 56.25% (20 Hz) showed decreased firing and 55% (10 Hz) and 43.75% (20 Hz) showed increased firing. Because the proportions of cells with excitatory and inhibitory responses were similar, there was no significant effect of optostimulation on the overall activity of mitral cells in the recorded population (Fig. 4F and Supplementary Fig. 5E). These results demonstrate that activation of LC–OB NAergic terminals bidirectionally modulates the activity of mitral cells.

Previous pharmacological studies have found that NE bidirectionally modulates the activity of mitral cells through changes to GABAergic transmission[38]. We therefore optogenetically activated LC–OB NAergic terminals and recorded sIPSCs from mitral cells (Supplementary Fig. 5F). Optostimulation (10-ms light pulses at 20 Hz for 1 min) decreased both the frequency and the amplitude of sIPSCs (Supplementary Fig. 5G, H).

Together, these results demonstrate that NE released from NAergic terminals in the OB bidirectionally modulates the excitability of mitral cells by altering inhibitory transmission.

Optostimulation of LC–aPC NAergic terminals decreases spontaneous and odor-evoked responses of aPC pyramidal neurons in vivo

Our whole-cell recordings demonstrate that optostimulation of NAergic terminals regulates the activity of aPC pyramidal neurons in vitro. We next investigated whether activation of NAergic terminals modulates aPC neural activity in vivo. We recorded extracellular single-unit activity of aPC pyramidal neurons in awake, head-fixed mice. To optogenetically activate NAergic terminals in the aPC, AAV-DIO-ChR2-eYFP virus was injected into the LC of DBH-Cre mice. After 3–4 weeks for viral expression, an op-microelectrode was implanted into layer 2/3 of the aPC to record extracellular single-unit spikes (Fig. 5A–C and Supplementary Fig. 6A, B). Spontaneous firing was suppressed after applying 20 Hz (Supplementary Fig. 6C, D), but not 10 Hz (Fig. 5D, E). These results

https://doi.org/10.1038/s41467-024-55609-9

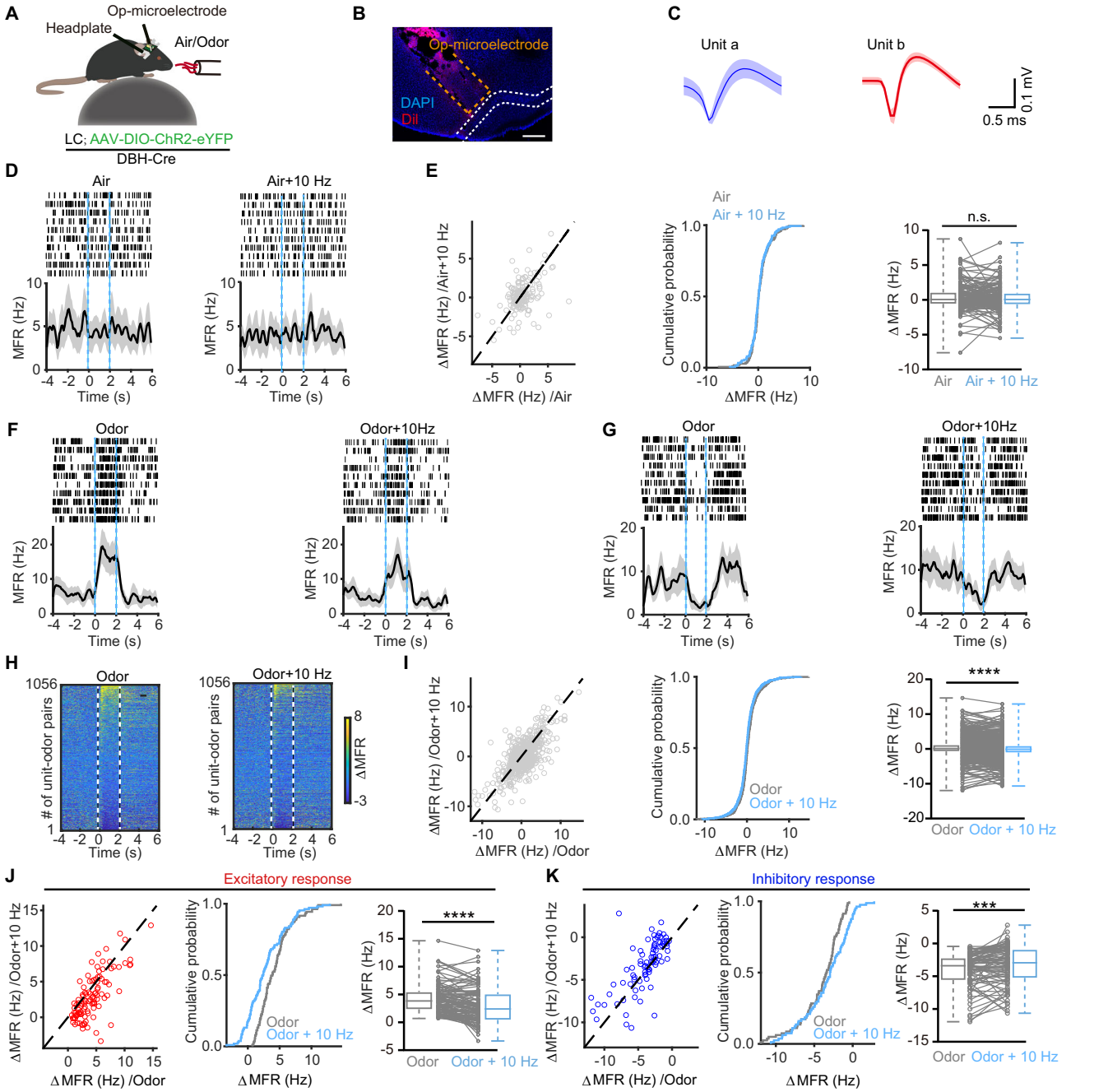

Fig. 5 | Optostimulation of LC–aPC NAergic terminals decreases the odor-evoked responses of aPC pyramidal neurons in vivo. A Schematic of the experiment. AAV-DIO-ChR2-eYFP virus was injected into the LC of DBH-Cre mice. **B** The position of the op-microelectrode implantation in the aPC (blue, DAPI; red, DiI; scale bars, 200 μm). **C** Example of spike sorting using PCA, with two units identified (unit a, blue; unit b, red). **D** Raster plots and mean firing rates (MFRs) in the absence and presence of laser stimulation. The blue dashed lines indicate the period of laser stimulation. **E** Optostimulation (10 Hz) had no effect on the ΔMFR of aPC pyramidal neurons ($p = 0.46$, $z = 0.73$, two-tailed Wilcoxon signed-rank test, $n = 176$ units from 17 mice). Odor-evoked excitatory responses (**F**) and inhibitory responses (**G**) in the presence and absence of 10-Hz optostimulation. The blue dashed lines indicate the period of combined odor and laser stimulation. **H** Heat maps of ΔMFR ($n = 1056$ unit–odor pairs from 17 mice). Each row represents one unit–odor pair ranked by the ΔMFR in light-off trials. **I** Optostimulation (10 Hz) reduced the overall odor-evoked responses ($p < 0.0001$, $z = 5.83$, two-tailed Wilcoxon signed-rank test, $n = 1056$ unit–odor pairs from 17 mice). Optostimulation (10 Hz) decreased the ΔMFR of excitatory responses (**J**; $p < 0.0001$, $z = 5.96$, two-tailed Wilcoxon signed-rank test, $n = 107$ unit–odor pairs from 17 mice) and increased the ΔMFR of inhibitory responses (**K**; $p = 0.0006$, $z = -3.43$, two-tailed Wilcoxon signed-rank test, $n = 81$unit–odor pairs from 17 mice). In (**E**, **I**, **J**, **K**), box-plots display median (center), upper and lower quartiles (box bounds) and whiskers representing minimum/maximum values. Data are presented as the means ± SEM (**C**, **D**, **F**, **G**). ***$p < 0.001$, ****$p < 0.0001$. ns no significance.

demonstrate that activation of NAergic terminals can decrease the spontaneous activity of aPC pyramidal neurons in awake mice.

To explore the effects of activation of LC–aPC NAergic terminals on odor-evoked activity of aPC pyramidal neurons, awake mice were presented with odors by a custom-built odor-delivery system. Similar to our previous findings in the OB[42,43], We observed both excitatory and inhibitory responses to odor delivery (Fig. 5F, G and Supplementary Fig. 6E, F). Figure 5H and Supplementary Fig. 6G show the effect of optostimulation (10-ms light pulses at 10 Hz or 20 Hz) on odor-evoked responses for all unit–odor pairs: in the population as a whole,

optostimulation (10 Hz and 20 Hz) led to a decrease in the odor-evoked firing rate of aPC pyramidal neurons (Fig. 5I and Supplementary Fig. 6H). We next analyzed the effect of optostimulation on odor-evoked excitatory and inhibitory responses, in more detail. Optostimulation (10 Hz and 20 Hz) of LC–aPC NAergic terminals decreased the odor-evoked firing rate of aPC pyramidal neurons with excitatory odor-evoked responses (Fig. 5J and Supplementary Fig. 6I), and only 10 Hz, but not 20 Hz, optostimulation increased the odor-evoked firing rate of inhibitory responses (Fig. 5K and Supplementary Fig. 6J). Therefore, overall, activation of LC–aPC NAergic terminals decreases odor-evoked responses in awake mice.

As a control, we performed the same experiment in DBH-Cre mice injected with AAV-DIO-eYFP virus into the LC. Optostimulation (10-ms light pulses at 20 Hz) had no effect on the spontaneous firing rate (Supplementary Fig. 7A) or odor-evoked responses (Supplementary Fig. 7B) in this eYFP control group.

Activation of LC–OB NAergic terminals decreases spontaneous and odor-evoked responses in M/Ts

To explore whether the LC–OB NAergic projection modulates the activity of mitral/tufted cells (M/Ts) in vivo, we recorded extracellular single-unit activity from M/Ts in awake, head-fixed mice. We injected AAV-DIO-ChR2-eYFP or AAV-DIO-eYFP virus into the LC of DBH-Cre mice and then implanted an op-tetrode/op-microelectrode into the OB (Fig. 6A–C and Supplementary Fig 8A, B). Optostimulation (10-ms light pulses) of LC–OB NAergic terminals at 20 Hz, but not 10 Hz, significantly reduced the spontaneous firing rate of M/Ts in the ChR2-eYFP group (Fig. 6D, E and Supplementary Fig. 8C, D).

We next evaluated whether optogenetic activation of NAergic terminals in the OB modulates odor-evoked activity in M/Ts. M/Ts displayed excitatory and inhibitory responses to odor stimulation (Fig. 6F, G and Supplementary Fig. 8E, F). Figure 6H (10 Hz) and Supplementary Fig. 8G (20 Hz) show the effect of optogenetic activation of NAergic terminals on the odor-evoked responses of M/Ts for all unit–odor pairs. Overall, optostimulation (10-ms light pulses) at 20 Hz, but not 10 Hz, decreased the odor-evoked firing of M/Ts in the recorded population (Fig. 6I and Supplementary Fig. 8H). We next analyzed the odor-evoked excitatory and inhibitory responses separately. We found that optostimulation (10 Hz and 20 Hz) decreased the odor-evoked firing rate of excitatory responses (Fig. 6J and Supplementary Fig. 8I) and increased the odor-evoked firing rate of inhibitory responses (Fig. 6K and Supplementary Fig. 8J). Optostimulation had no effect on the spontaneous (Supplementary Fig. 7C) or odor-evoked (Supplementary Fig. 7D) responses of M/Ts in the eYFP control group. Therefore, these data indicate that activation of LC–OB NAergic terminals decreases both spontaneous and odor-evoked responses in M/Ts.

Activation of LC–aPC/OB NAergic terminals increases the odor-decoding performance in the aPC but decreases it in the OB

Neural decoding can be used to evaluate how well neural responses can discriminate between different odors. To investigate the role of the LC–aPC/OB circuits in the neural decoding of odor information, we used a support vector machine (SVM) to assess the classification of any two odors among all odors. Figure 7A, B show the extraction and combination of classification features. Figure 7C, D show that activation of the LC–aPC NAergic pathway increased the odor-decoding ability of the aPC. Contrary to the results for the aPC, activation of the LC–OB NAergic terminals significantly decreased the odor-decoding performance in the OB (Fig. 7E, F). Therefore, activation of NAergic terminals significantly increases the odor-decoding ability in the aPC but decreases it in the OB.

Optogenetic but not chemogenetic activation of the LC–aPC/OB circuit regulates difficult odor discrimination

The results obtained from our in vivo and in vitro experiments consistently indicate that LC NAergic neurons play a critical role in the modulation of neural activity in the aPC and OB. This prompted us to explore whether modulation of LC–aPC/OB projections affects olfactory behaviors. We injected AAV-retro-Cre virus bilaterally into the aPC/OB and AAV-DIO-hM3D-mCherry or AAV-DIO-mCherry virus into bilateral LC in C57BL/6J mice to chemogenetically activate the LC–aPC/OB circuits during an olfactory behavioral task (Supplementary Fig. 9A). Clozapine-N-oxide (CNO; 3 mg/kg, i.p.) or saline was administrated daily to the experimental group (hM3D-CNO) and the control groups (hM3D-saline, mCherry-CNO) 30–40 minutes before the experiment. Mice were trained on the go/no-go olfactory discrimination task (Supplementary Fig. 9B). First (Days 1 to 2), mice were trained to lick the water tube within a 2-s time window after the start of odor delivery to obtain a water reward (go/go task). Then for the go/no-go task (Days 3 to 9), mice were trained to discriminate two easy odors (Days 3 to 5; S + : isoamyl acetate; S − : 2-heptanone) and then two difficult odors (Days 6 to 9; S + : isoamyl acetate: 2-heptanone = 3:2; S − : 2-heptanone: isoamyl acetate = 3:2) to receive the water reward. One of the odors was rewarded upon licking (S + , go) whereas the other was not (S − , no-go). The mice learned to lick the tube in response to the S+ (Hit) and to withhold licking when the S− was presented (correct rejection, CR). Both Hits and CRs were deemed correct responses, whereas Misses (failing to lick in response to the S +) and false alarms (FAs; licking in response to the S −) were deemed incorrect responses. The performance of mice in the go/no-go task was calculated for Days 3 to 9 as the percentage of Hits plus CRs relative to the total number of trials (accuracy). There were no differences in the total accuracy, training intensity or accuracy of CRs between the experimental group and the control groups (Supplementary Fig. 9C–E). The accuracy of Hits was slightly worse in the experimental group than in the control groups (Supplementary Fig. 9F). These results demonstrate that chemogenetic activation of the LC–aPC/OB pathway has no effect on olfactory discrimination. We next investigated the influence of activation of the LC–aPC/OB NAergic pathway on olfactory detection. There were no differences between the experimental group and the control groups in either the buried food pellet test (Supplementary Fig. 9G) or the visible food pellet test (Supplementary Fig. 9H). Therefore, chemogenetic activation of the LC–aPC/OB pathway has no effect on olfactory detection.

To rule out the possibility that our above negative results were due to the long duration of activation of LC NAergic neurons that occurs with chemogenetics, we instead optogenetically activated (473 nm, 10-ms pulse, 10 Hz) the LC–aPC/OB projections by expressing ChR2-eYFP in LC NAergic neurons and delivering light via optical fibers implanted in the aPC and OB while mice performed the go/no-go test (Fig. 8A, B). The mice received 10-Hz blue light pulses (10 ms) during the 2-s odor-delivery window. The performance of mice in the go/no-go task was calculated for Days 3 to 9 as the percentage of Hits plus CRs relative to the total number of trials (accuracy). Activation of the LC–aPC/OB circuit significantly increased accuracy in the experimental group compared with the control animals in the difficult version (Fig. 8C). There was no significant difference in training intensity between the ChR2-eYFP group and the eYFP group (Fig. 8D), indicating that the difference in accuracy was not due to differences in training intensity. We also analyzed the accuracy of Hits and CRs separately. We found that the accuracy of CRs (Fig. 8E) but not Hits (Fig. 8F), was better in the ChR2-eYFP group than the eYFP group, indicating that an increase in correct rejections on the S− trials was responsible for the enhanced odor discrimination in the ChR2-eYFP group. These results demonstrate that optogenetic activation of the LC–aPC/OB NAergic circuit accelerates odor discrimination when the task is relatively difficult.

https://doi.org/10.1038/s41467-024-55609-9

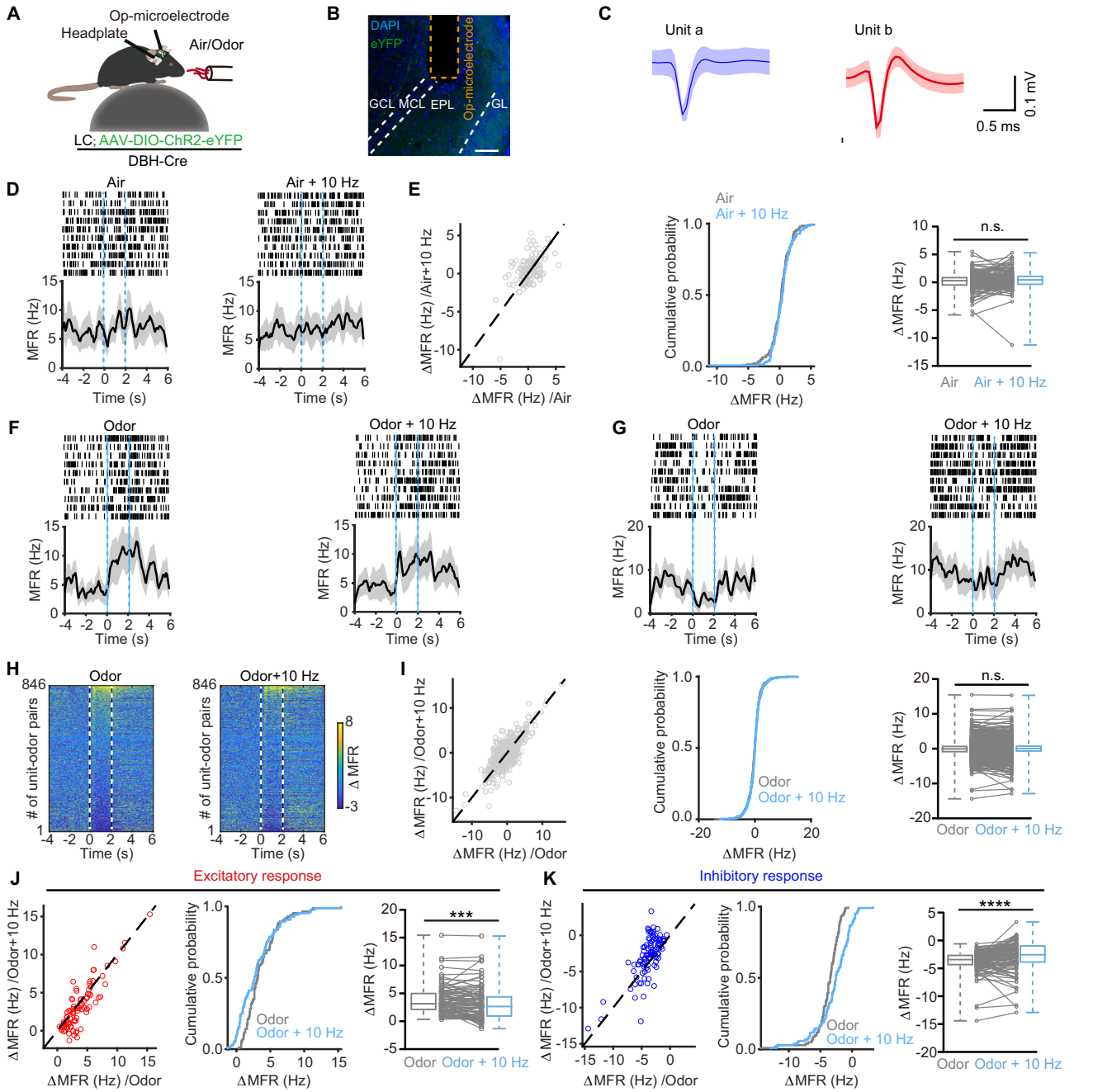

Fig. 6 | Optostimulation of LC–OB NAergic terminals decreases the odor-evoked responses of M/Ts in vivo. A Schematic of the experiment. AAV-DIO-ChR2-eYFP virus was injected into the LC of DBH-Cre mice. **B** The position of the op-microelectrode in the OB (blue, DAPI; green, eYFP; scale bar, 100 μm). **C** Example of spike sorting by PCA, with two units identified (unit a, blue; unit b, red). **D** Raster plots and MFR in the presence and absence of optostimulation. Dashed blue lines indicate the laser stimulation period. **E** Optostimulation (10 Hz) of NAergic terminals had no effect on the ΔMFR of M/Ts ($p = 0.20$, $z = -1.29$, two-tailed Wilcoxon signed-rank test, $n = 141$ units from 13 mice). Odor-evoked excitatory (**F**) and inhibitory (**G**) responses in the presence and absence of optostimulation. Dashed blue lines indicate the period of combined odor and laser stimulation. **H** Heat maps of ΔMFR ($n = 846$ unit–odor pairs from 13 mice). **I** Optostimulation (10 Hz) had no effect on the overall odor-evoked response ($p = 0.12$, $z = -1.55$, two-tailed Wilcoxon signed-rank test, $n = 846$ units from 13 mice). Optostimulation (10 Hz) of NAergic terminals reduced the ΔMFR of excitatory responses (**J**; $p = 0.00013$, $z = 3.83$, two-tailed Wilcoxon signed-rank test, $n = 85$ units from 13 mice) but increased the ΔMFR of inhibitory responses (**K**; $p < 0.0001$, $z = -4.89$, two-tailed Wilcoxon signed-rank test, $n = 102$ units from 13 mice). In (**E**, **I**, **J**, **K**), boxplots display median (center), upper and lower quartiles (box bounds) and whiskers representing minimum/maximum values. Data are presented as the means ± SEM (**C**, **D**, **F**, **G**). ***$p < 0.001$, ****$p < 0.0001$. ns no significance.

Chemogenetic suppression of LC NAergic neurons impairs olfactory detection, odor preference, and discrimination

After conducting the above gain-of-function behavioral experiments, we next carried out loss-of-function behavioral experiments. We next explored whether chemogenetic inactivation of LC NAergic neurons affects olfactory behaviors. To do this, we injected AAV-DIO-hM4D-mCherry into the LC of DBH-Cre mice (Supplementary Fig. 10A). Whole-cell recording in vitro confirmed that CNO (10 μM) decreased the frequency of spontaneous spiking and the RMP in LC hM4D-expressing NAergic neurons, indicating that this manipulation efficiently inhibits LC NAergic neurons (Supplementary Fig. 10B, C).

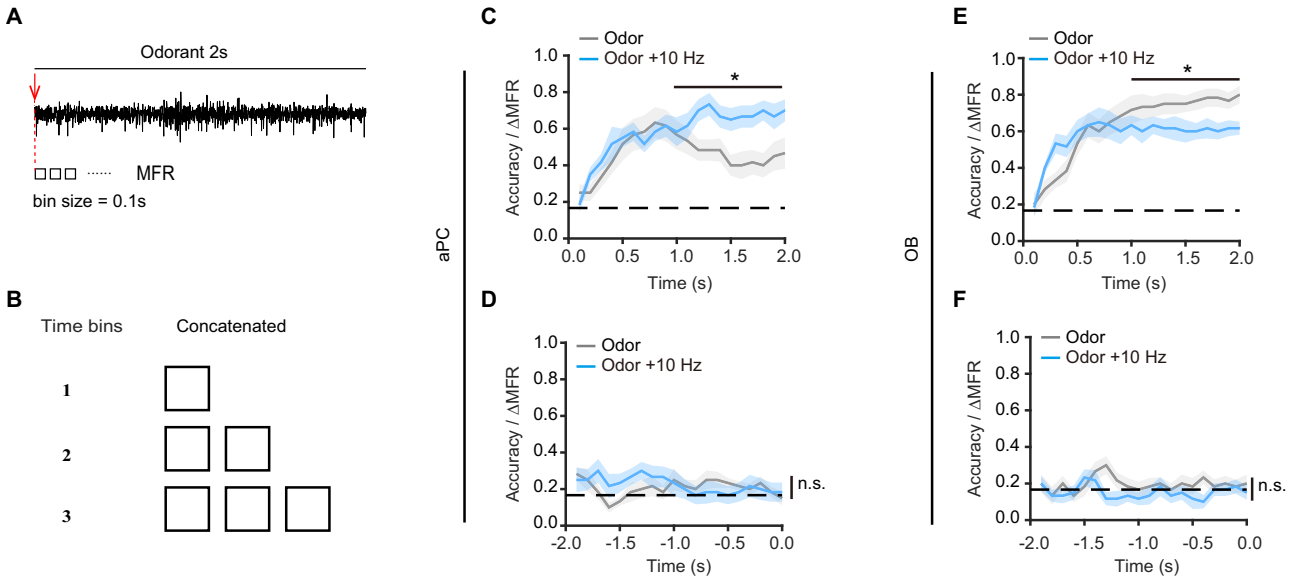

Fig. 7 | Optostimulation of LC–aPC/OB terminals increases the odor-decoding performance of the aPC but decreases the odor-decoding performance of the OB. A Schematic of the extraction pattern of classification features used for odor decoding. Classification features were created by binning spike counts into 0.1-s bins. **B** Testing and training data consisted of incrementally concatenated 0.1-s non-overlapping bins from 0 to t. **C**–**F** The classification accuracy of a support vector machine model for distinguishing different odorants (gray, odor; blue, odor + 10 Hz), where the black dotted line represents the chance level (1/6). Performance for the aPC (**C**: $p = 0.015$, $F_{(1,18)} = 7.25$; **D**: $p = 0.69$, $F_{(1,18)} = 0.16$; two-way ANOVA, $n = 176$ units from 17 mice) and the OB (**E**: $p = 0.030$, $F_{(1,18)} = 5.57$; **F**: $p = 0.21$, $F_{(1,18)} = 1.67$; two-way ANOVA, $n = 141$ units from 13 mice). −2–0 s: no odor stimulation and no optostimulation; 0–2 s: the odor stimulation period in the presence or absence of optostimulation. Data are presented as the means ± SEM *$p < 0.05$, ns no significance.

To test whether inactivation of LC NAergic neurons affects olfactory discrimination, we again conducted the go/no-go test. CNO or saline was administrated daily (3 mg/kg, i.p.) to the experimental group (hM4D-CNO) and the control group (hM4D-saline) 30–40 min before the experiment. The performance of mice in the go/no-go task was calculated for Days 3 to 5 as the percentage of Hits plus CRs relative to the total number of trials (accuracy). The accuracy of the hM4D-CNO group was lower than the accuracy of the hM4D-saline group (Supplementary Fig. 10E). There was no significant difference in training intensity between the hM4D-CNO group and the hM4D-saline group, indicating that the difference in accuracy was not due to differences in training intensity (Supplementary Fig. 10F). We also analyzed the accuracy of Hits and CRs separately. We found that the accuracy of CRs, but not Hits, was worse in the hM4D-CNO group than the hM4D-saline group, indicating that a reduction in correct rejections on the S− trials was responsible for the impaired odor discrimination in the hM4D-CNO group (Supplementary Fig. 10G, H). These results demonstrate that inactivation of LC NAergic neurons impairs olfactory discrimination.

To further investigate the influence of inactivation of LC NAergic neurons on olfactory detection, we conducted the buried pellet test. The hM4D-CNO group took longer to retrieve a buried food pellet than the hM4D-saline group (Supplementary Fig. 10I). There was no difference between the two groups when the food pellet was visible, indicating that CNO injection in the hM4D mice did not cause any changes in vision or mobility compared with the hM4D-saline group (Supplementary Fig. 10J). These results demonstrate that inactivation of LC NAergic neurons impairs olfactory detection.

We next explored the effect of inactivation of LC NAergic neurons on innate olfactory preference and avoidance. Mice performed an olfactory preference/avoidance test in a custom-designed test chamber (Supplementary Fig. 10K). As in our previous studies[42], peanut butter and 2,4,5-trimethylthiazole (TMT) were used as attractant and aversive odorants, respectively. We measured how long the mice spent investigating a cotton swab containing one of these odorants versus mineral oil to assess preference and avoidance. In the preference test, the control hM4D-saline group spent more time in the chamber with the peanut butter odorant than the chamber with the mineral oil, whereas the hM4D-CNO group had no preference for either chamber (Supplementary Fig. 10L). The real-time place preference (RTPP) index was slightly lower in the hM4D-CNO group than the hM4D-saline group (Supplementary Fig. 10M). In the avoidance test, both groups spent less time in the chamber with the TMT than the chamber with the mineral oil (Supplementary Fig. 10N), and there was no significant difference between the two groups in the RTPP index (Supplementary Fig. 10O). These results indicate that inactivation of NAergic neurons impaired innate olfactory preference, but not innate olfactory avoidance.

To explore the effect of inactivation of LC NAergic neurons on anxiety-like behavior and mobility, we assessed the behavior of mice in the open-field test. There were no differences between the hM4D-CNO group and the hM4D-saline group in the total distance traveled or the total center distance (Supplementary Fig. 10P), indicating that inactivation of LC NAergic neurons did not affect mobility or anxiety-like behavior.

Together, these results confirm that LC NAergic neurons are necessary for olfactory detection, odor preference, and odor discrimination.

Chemogenetic inhibition of the LC–aPC/OB circuit impairs olfactory detection and odor discrimination

The above results demonstrate that inactivation of LC NAergic neurons impairs olfactory behaviors. We speculated that these effects may be occurring via the LC–aPC/OB NAergic pathway. To chemogenetically inhibit the LC–aPC/OB pathway, we injected AAV-retro-Cre virus bilaterally into the aPC and OB and AAV-DIO-hM4D-mCherry or AAV-DIO-mCherry virus into bilateral LC in C57BL/6J mice (Fig. 8G). After waiting 4 weeks for viral expression, immunohistochemistry confirmed that hM4D-mCherry was expressed specifically in LC NAergic neurons (Fig. 8H, I). Whole-cell recordings in vitro confirmed that CNO (10 μM) decreased the membrane potential and the frequency of spontaneous spiking in LC hM4D-mCherry$^+$ neurons (Fig. 8J–L).

https://doi.org/10.1038/s41467-024-55609-9

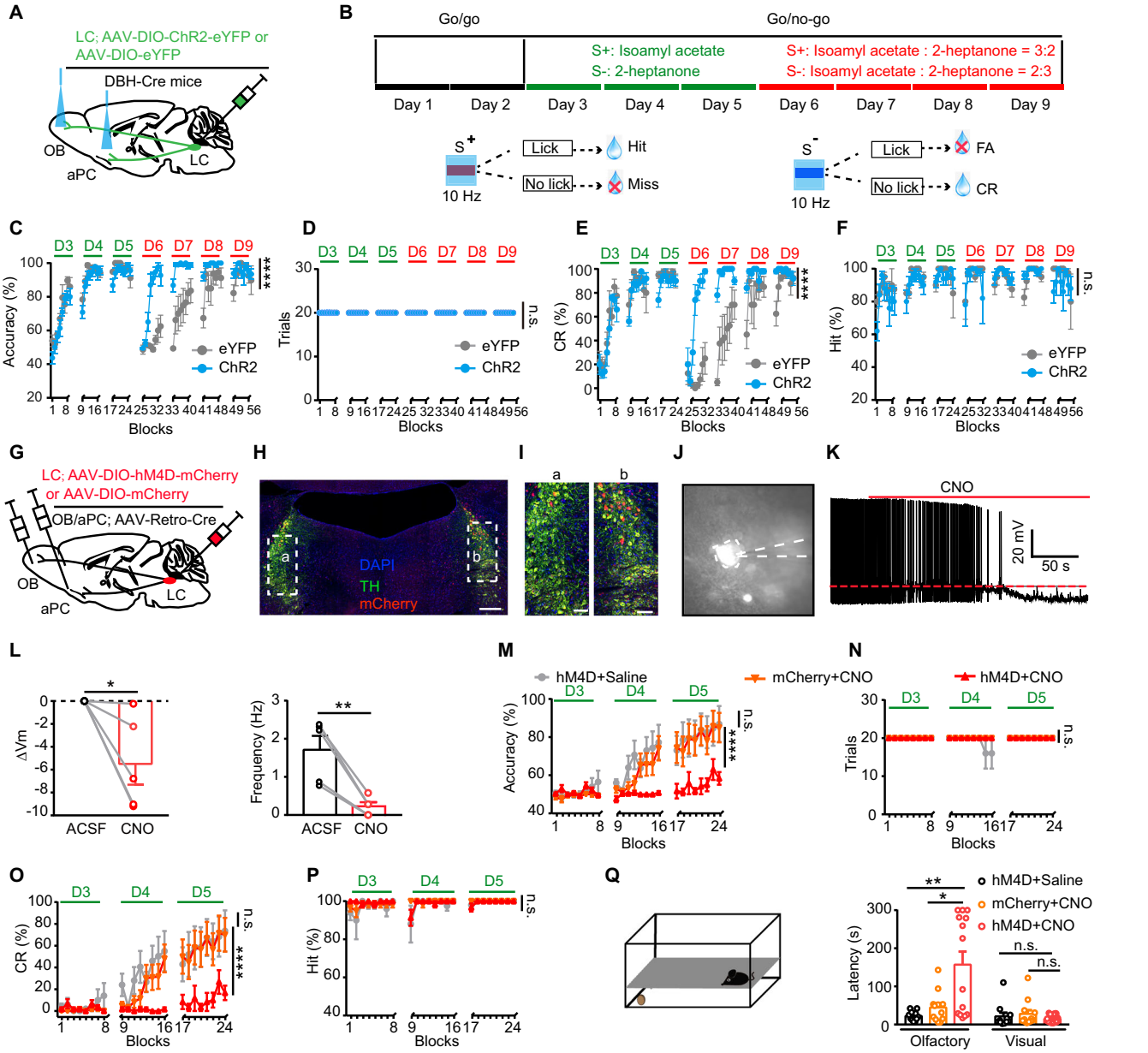

Fig. 8 | Optogenetic activation and chemogenetic suppression of the LC–aPC/OB NAergic pathway bidirectionally regulate odor discrimination. Schematic of the virus injections (**A**) and the go/no-go task (**B**). **C** Accuracy in the go/no-go task ($p < 0.0001$, $F(1, 392) = 108.40$; two-way ANOVA; ChR2-eYFP, n = 5 mice; eYFP, n = 4 mice). **D** The total number of trials during the go/no-go task ($p > 0.99$, $F_{(1, 447)} = 0.00$; two-way ANOVA; ChR2-eYFP, n = 5 mice; eYFP, n = 4 mice). **E** CR accuracy ($p < 0.0001$; $F_{(1, 392)} = 134.40$; two-way ANOVA; ChR2-eYFP, n = 5 mice; eYFP, n = 4 mice). **F** Hit accuracy ($p = 0.10$; $F_{(1, 392)} = 2.66$; two-way ANOVA; ChR2-eYFP, n = 5 mice; eYFP, n = 4 mice). **G** Schematic of the virus injections. **H** IHC revealed co-labeling of TH staining with hM4D-mCherry$^+$ neurons in the LC. Blue, DAPI; green, TH; red, mCherry; scale bar, 100 μm. **I** Magnification of the areas indicated in (**H**). Scale bar, 25 μm. **J** Sample image of whole-cell recording of an hM4D-mCherry$^+$ neuron. **K** Raw trace showing spontaneous firing before and after application of CNO. **L** Quantitative analysis of the change in membrane potential (ΔVm) ($p = 0.039$, $t_{(4)} = 3.02$, two-sided paired t-test; n = 5 from 3 mice) and frequency of spontaneous firing ($p = 0.0059$, $t_{(4)} = 5.35$, two-sided paired t-test, n = 5 cells from 3 mice). **M** Accuracy in the go/no-go task (hM4D-saline versus mCherry-CNO, $p = 0.073$, $q = 3.11$; hM4D-saline versus hM4D-CNO, $p < 0.0001$; $q = 14.04$; mCherry-CNO versus hM4D-CNO, $p < 0.0001$, $q = 11.53$; two-way ANOVA; hM4D-saline, n = 5 mice; mCherry-CNO, n = 6 mice; hM4D-CNO, n = 6 mice). **N** The total number of trials during the go/no-go task (hM4D-saline vs mCherry-CNO, $p = 0.13$, $q = 2.76$; hM4D-saline vs hM4D-CNO, $p = 0.13$, $q = 2.76$; mCherry-CNO vs hM4D-CNO, $p > 0.99$, $q = 0.00$; two-way ANOVA; hM4D-saline, n = 5 mice; mCherry-CNO, n = 6 mice; hM4D-CNO, n = 6 mice). **O** CR accuracy (hM4D-saline vs mCherry-CNO, $p = 0.079$, $q = 3.06$; hM4D-saline vs hM4D-CNO, $p < 0.0001$, $q = 13.99$; mCherry-CNO vs hM4D-CNO, $p < 0.0001$, $q = 11.53$; two-way ANOVA; hM4D-saline, n = 5 mice; mCherry-CNO, n = 6 mice; hM4D-CNO, n = 6 mice). **P** Hit accuracy (hM4D-saline vs mCherry-CNO, $p = 0.28$, $q = 2.15$; hM4D-saline vs hM4D-CNO, $p = 0.19$, $q = 2.46$; mCherry-CNO vs hM4D-CNO, $p = 0.97$, $q = 0.33$; two-way ANOVA, hM4D-saline, n = 5 mice; mCherry-CNO, n = 6 mice; hM4D-CNO, n = 6 mice). **Q** Schematic of the buried pellet test and quantitative analysis of the time to find the buried pellet (hM4D-saline vs hM4D-CNO, $p = 0.0020$, $z = 3.08$; mCherry-CNO vs hM4D-CNO, $p = 0.049$, $z = 1.97$; Kruskal–Wallis test, hM4D-saline, n = 11 mice; mCherry-CNO, n = 12 mice; hM4D-CNO, n = 14 mice) and the visible pellet (hM4D-saline vs hM4D-CNO, $p = 0.69$, $z = 0.39$; mCherry-CNO vs hM4D-CNO, $p = 0.42$, $z = 0.81$; Kruskal-Wallis test; hM4D-saline, n = 11 mice; mCherry-CNO, n = 12 mice; hM4D-CNO, n = 14 mice). Data are presented as the means ± SEM. *p < 0.05, **p < 0.01, ****p < 0.0001. ns no significance.

We next investigated the influence of inactivation of the LC–aPC/OB NAergic pathway on olfactory behaviors. CNO (3 mg/kg, i.p.) or saline was administrated daily to the experimental group (hM4D-CNO) and the control groups (hM4D-saline, mCherry-CNO) 30–40 min before the experiment. First, we used the go/no-go task to explore olfactory discrimination. The performance of mice in the go/no-go task was calculated from Days 3 to 5. The accuracy (the percentage of Hits plus CRs relative to the total number of trials) of the experimental group was significantly lower than the accuracy of the control groups (Fig. 8M) and there were no significant differences in training intensity between the experimental group and the control groups (Fig. 8N). We next analyzed the accuracy of Hits and CRs separately. The accuracy of CRs, but not Hits, was worse in the experimental group than in the control groups (Fig. 8O, P). These results demonstrate that inactivation of the LC–aPC/OB pathway impairs olfactory discrimination.

We next investigated the influence of inactivation of the LC–aPC/OB NAergic pathway on olfactory detection. In the buried pellet test, the experimental group took more time to retrieved the buried pellet than the control groups, but there were no differences between groups when the food pellet was visible (Fig. 8Q). Therefore, inactivation of the LC–aPC/OB pathway impairs olfactory detection.

Interestingly, compared with inactivation of LC NAergic neurons, inactivation of the LC–aPC/OB NAergic pathway resulted in slightly more robust behavioral changes (Supplementary Fig. 10E, G, I vs. Figure 8M, O, Q). Although it is likely that a greater number of NAergic neurons were inactivated by the non-specific manipulation, some of these neurons likely did not project to the aPC/OB. The non-specific manipulation may therefore have attenuated the effect of LC NAergic neurons on the olfactory system through complex effects on neural networks in the wider brain: LC NAergic neurons are known to have extensive effects across almost the whole brain.

We also explored the influence of inactivation of the LC–aPC/OB NAergic circuit on innate olfactory preference and avoidance. In the innate olfactory preference test (Supplementary Fig. 11A), the experimental group and the control groups spent more time in the chamber with the peanut butter odor than the chamber with mineral oil (Supplementary Fig. 11B), and there was no difference in the RTPP index (Supplementary Fig. 11C). In the innate olfactory avoidance test (Supplementary Fig. 11D), the experimental group and the control groups showed avoidance of TMT (Supplementary Fig. 11E), and there was no difference in the RTPP index (Supplementary Fig. 11F). Therefore, inactivation of the LC–aPC/OB NAergic pathway has no effect on innate olfactory preference or avoidance.

Finally, in the open-field test (Supplementary Fig. 11G), there were no differences in the total distance traveled (Supplementary Fig. 11H) or total center distance (Supplementary Fig. 11I) between the experimental group and the control groups, indicating that inactivation of the LC–aPC/OB NAergic pathway has no effect on mobility or anxiety-like behavior.

Altogether, these results indicate that inactivation of the LC–aPC/OB NAergic pathway attenuates olfactory detection and odor discrimination.

Inhibition of the LC–aPC pathway, but not the LC–OB pathway, impairs odor discrimination in a go/no-go task

The above results indicate that loss-of-function of the LC–aPC/OB NAergic circuits produces deficits in olfactory processing. The morphological results indicate that more LC NAergic neurons project to the aPC than the OB. This prompted us to investigate the separate contribution of the LC–aPC and LC–OB NAergic projections to olfactory behaviors. To specifically inhibit the LC–aPC or LC–OB pathways, AAV-retro-Cre virus was bilaterally injected into the aPC or the OB and AAV-DIO-hM4D-mCherry virus was injected into bilateral LC in C57BL/6 J mice (Supplementary Fig. 12A, G). CNO (3 mg/kg, i.p.) or saline was administrated daily to the experimental group (hM4D-CNO) and the control groups (hM4D-saline) 30–40 min before the go/no-go task. The performance of mice in the go/no-go task was calculated from Days 3 to 9. Inhibition of the LC NAergic projection to the aPC resulted in significant decreases in total accuracy (Supplementary Fig. 12B) and in the accuracy of CRs (Supplementary Fig. 12C). There were no significant differences in Hits (Supplementary Fig. 12D) or training intensity (Supplementary Fig. 12E) between the experimental group and the control groups. Unlike the effects with the LC–aPC pathway, inhibition of the LC NAergic projection to the OB had no effect on odor discrimination (Supplementary Fig. 12H–K). There was no effect on performance in the buried pellet test with inhibition of either the LC–aPC pathway or the LC–OB pathway (Supplementary Fig. 12F, L).

Discussion

In this study, we investigated the mechanism by which LC NAergic neurons modulate the aPC/OB and demonstrated the role of the LC–aPC/OB pathways in odor representation and olfactory behaviors. Our results show that LC NAergic neurons project directly to the aPC and the OB. Furthermore, NE (released synaptically or applied exogenously) reduces the excitability of aPC pyramidal neurons via α2 receptors and bidirectionally modulates the activity of OB mitral cells through changes to inhibitory transmission. Functionally, this NAergic projection modulates odor-evoked responses and odor-decoding in the aPC/OB. Optogenetic activation and chemogenetic suppression of the LC–aPC/OB NAergic pathway bidirectionally regulate odor discrimination. Therefore, these findings provide direct evidence for the involvement of the LC NAergic pathway in olfactory information processing and representation.

Both the OB and the aPC have a multi-layer structure, and each layer contains different types of neurons[44–46]. Although previous studies have revealed that LC neurons project to the OB and the aPC[20,21,30,31], the details of how the LC NAergic projection acts at the synaptic level in the aPC/OB has remained largely unknown. Furthermore, although both of these olfactory brain centers receive a NAergic projection from the LC, whether neurons in the OB and the aPC receive projections from the same or different LC neurons also remained elusive. With a combination of retrograde and anterograde viral labeling methods, we provide evidence that LC NAergic neurons project directly to each layer of the aPC and the OB. Interestingly, most LC–OB projecting NAergic neurons also project to the aPC; however, only a few of the LC–aPC projecting NAergic neurons also project to the OB, indicating that the LC–aPC NAergic projection may play a more important role in modulating olfactory processing. Thus, our present study provides interesting findings about the projection patterns from the LC to the aPC/OB, and the results represent a first step toward understanding the anatomical details and underlying neural mechanisms by which these olfactory centers are modulated by LC NAergic neurons.

At the synaptic level, NAergic input to the OB bidirectionally modulates the activity of mitral cells whereas NAergic input to the aPC predominantly reduces the excitability of aPC pyramidal neurons via α2 receptors. Therefore, although LC NAergic neurons project to both the OB and the aPC, the projection patterns and underlying mechanisms are strikingly different. These findings suggest that LC NAergic neurons modulate the olfactory centers via different modes, which is supported by previous studies showing that the OB and the aPC represent odor information via different strategies[1,9].

Although brain modulatory systems contain a very limited number of neurons, they can innervate many brain regions from the OB to the cerebellum and contribute to a variety of functions[18,19]. One reason for this is their branching axons that project simultaneously to multiple brain regions. For example, individual pontine-tegmental cholinergic neurons send abundant collaterals to multiple targets in both hemispheres[47]. Similarly, LC NAergic neurons can project to both the forebrain and the cerebellum simultaneously[41]. Interestingly, we

observed this branching NAergic projection pattern for the OB/aPC, with some individual neurons projecting to both the OB and the aPC, although others projected only to the aPC. Although we did not observe differences in the electrophysiological characteristics of these two types of NAergic neuron, it is likely that this projection pattern is important for olfactory information processing in the central olfactory system.

When investigating the extent to which LC neurons project to the OB and aPC, we sampled only a portion of the total population of LC neurons because of technical limitations. It is likely that such sampling indirectly reflects the real situation; however, because some neurons projecting to the OB/aPC may have remained unlabeled in the LC owing to variability in viral expression, the percentages presented may be underestimates and may not reflect the true proportions. Likewise, incomplete viral expression may have affected our categorization of LC projection neurons into two types. From our data, we identified type I LC neurons, which project to both the aPC and the OB, and type II LC neurons, which project only to the aPC. However, we cannot exclude the possibility that type II neurons may actually project to the OB as well but that this was missed owing to variability in the expression of the virus. Overall, although our data indicate the number and percentage of LC–OB/aPC neurons and suggest that two main types of LC–OB/aPC projection neurons exist, further studies using better labeling and imaging techniques will be required to confirm these observations in the future.

The widespread distribution of NAergic fibers and receptors underlies the diverse physiological functions of NE. NE regulation of neural excitability varies with its concentration and receptor subtypes[33,38]. NE usually increases neuronal excitability by directly activating α1 or β receptors and decreases neuronal excitability by activating α2 receptors[48]. In the aPC, previous studies have shown the existence three NAergic receptors subtypes (α1, β, and α2) in layer 2[34]. Different concentrations of exogenous NE have been found to alter pre- and postsynaptic excitatory and inhibitory transmission in aPC pyramidal neurons in younger mice (p8–14) through activation of β or α receptors, suggesting that NE can excite or inhibit aPC pyramidal neurons[37]. Our in vitro electrophysiological results demonstrated that exogenous NE application decreased the excitability of aPC pyramidal neurons by activating α2 receptors, which was further confirmed by optogenetic activation of aPC NAergic terminals. This α2-mediated regulatory mechanism has been observed in other brain regions, such as the ventrolateral preoptic area[22].

As a classic method, pharmacological application of NE is easy to manipulate, although the NE is exogenous. Optogenetic stimulation of LC NEergic neurons causes endogenous release of NE, which is closer to physiological conditions. Thus, in present study, we used both strategies to investigate systematically how LC NAergic neurons modulate neural activity in the aPC/OB. The comparison between pharmacological and optogenetic manipulations may provide important information for researchers who prefer to use exogenous application of NE. In addition, we found that some pyramidal neurons showed increased firing to optostimulation, that was not blocked by α2 receptor blockers. This may be explained by differential co-expression of other types of NE receptors on aPC pyramidal neurons. Overall, although previous studies have investigated how exogenous application of NE affects the excitability of aPC pyramidal neurons, our comparison of exogenous NE application and optogenetically evoked endogenous NE release provides consistent data to show that LC–aPC NAergic projections mainly inhibit aPC pyramidal neurons directly via α2 receptors.

In the OB, because of the varying distribution and affinities of NE receptor subtypes and the complexity of the circuit connections, the effect of NE regulation on mitral cell activity remains controversial. Mitral cells express three NE receptors (α1, α2, and β), and granule cells express α1 and α2 receptors[32,33]. In addition, NAergic fibers preferentially target the granule cell layer, and to a lesser extent the mitral cell layer[31]. Thus, most studies suggest that NE modulates GABAergic inhibition of mitral cells by activating/inhibiting granule cells. High levels of NE facilitate inhibition of M/Ts via activation of α1 receptors on granule cells, whereas low doses of NE facilitate excitation of M/Ts via α2-mediated inhibition of granule cells[38,49]. These previous pharmacological results are further confirmed by our finding that synaptically released NE (induced by optostimulation) indirectly modulates the activity of mitral cells in a bidirectional manner through inhibitory transmission. Since mitral cells also express three types of adrenergic receptors, direct modulation is also likely. A previous study found that NE directly regulates the activity of mitral cells via activation of α1 receptors[50]. Further studies are required to investigate whether activation of NAergic terminals directly regulates the excitability of mitral cells in this manner.

The functional significance of NAergic modulation of aPC/OB activity is elusive, although a few studies have shed some light on the issue. For example, a previous study found that electrical stimulation of the LC under anesthesia increased odor-evoked responses in the aPC but decreased odor-evoked responses of M/Ts[35,36]. Interestingly, our in vivo electrophysiological results showed that optogenetic activation of NAergic terminals significantly inhibited the spontaneous and odor-evoked responses of both aPC pyramidal neurons and OB M/Ts in awake head-fixed mice. It is likely that this discrepancy in results for the aPC is due to the different stimulation methods. The LC contains not only NAergic neurons but also a few GABAergic neurons[51,52]; optostimulation specifically activates NAergic neurons whereas electrical stimulation has no selectivity. More functionally importantly, our results suggest that LC NAergic neurons modulate the odor-decoding ability of the aPC/OB, a function that is required to identify and discriminate odor information. Therefore, the LC–aPC/OB pathway is critically involved in modulating the neural output of the aPC/OB. This functional speculation is supported by the results from our behavioral tests: chemogenetic inhibition of either LC NAergic neurons or the LC NAergic projections to the aPC and OB impaired odor discrimination and odor detection. Simultaneous chemogenetic inhibition of both the LC-aPC and LC-OB pathways leads to a pronounced behavioral change, even more significant than inhibiting all LC neurons together. This suggests that targeted manipulation of LC-aPC/OB NAergic neurons plays a more crucial role in regulating olfactory behaviors compared to non-specific LC neuron inhibition. Interestingly, while the combined inhibition of the LC-aPC/OB pathways induces significant behavioral changes, inhibiting either the LC-aPC or LC-OB pathway individually results in only weak (LC-aPC) or no (LC-OB) effects. There are two potential explanations for these observations. First, the number of inhibited LC NAergic neurons varies between these pathways. Data from our viral labeling strategy indicates that a larger number of LC-aPC/OB NAergic neurons were inhibited, with LC-aPC neurons being more affected than LC-OB neurons. This difference in the number of inhibited neurons likely accounts for the observed behavioral differences. Second, as indicated in this study, at least two types of LC NAergic neurons project to the aPC and OB. LC neurons projecting to the OB are primarily type I, whereas those projecting to the aPC include both type I and type II neurons. These specific projections might also have distinct functional roles, contributing to the differences in behavioral outcomes. In contrast to the chemogenetic inhibition experiments, optogenetic activation of the LC-aPC/OB circuit enhanced olfactory discrimination, whereas chemogenetic activation did not produce the same effect. This difference can be attributed to the distinct firing patterns of LC NAergic neurons, which can fire in either phasic or tonic modes, each leading to different functional outcomes. Chemogenetic activation tends to mimic tonic firing, while the optogenetic activation used in the Go/no-go experiment more closely resembles phasic firing. Our findings are supported by a recent study that found phasic, but not tonic, LC activity enhances odor discrimination learning[27]. Thus, the divergent effects of these two activation methods on olfactory discrimination can be explained by the differences in the neuronal firing patterns they induce. Additionally,

although we did not observe significant changes in olfactory behaviors when activating the LC-OB or LC-aPC pathways separately, it is likely that separate optogenetic activation of these pathways would produce weaker effects, or none at all, compared to simultaneous activation, due to the number and types of NAergic neurons involved. Consistent with our findings, a recent study showed that distinct LC activation patterns differentially modulate olfactory behaviors, indicating that LC NAergic neurons participate in the regulation of olfactory function[27]. Furthermore, previous pharmacological studies have demonstrated that NE has a variety of effects on odor processing in the OB and the aPC, such as modulating odor preference, odor detection, odor discrimination, and olfactory thresholds[37,39,40,53]. In addition, it is well established that LC NAergic neurons plays important roles in the regulation of brain states, including arousal, attention, and anxiety[22,54,55]. This raises the question of whether inactivation of LC NAergic neurons regulates olfactory function indirectly through an effect on brain state. However, this possibility can be at least partially ruled out since the behavioral performance of the mice in the open-field test was unchanged.

In summary, the present study identifies the anatomical connections and synaptic mechanisms by which LC NAergic neurons regulate the activity of the aPC and the OB and the functional significance of this modulation in odor representation and olfactory behaviors. These findings are important for understanding the role of the NAergic system in olfaction and how the central olfactory system is modulated by centrifugal inputs.

Methods

Animals

DBH-Cre and C57BL/6J mice were used in our experiments. The mice were group housed and maintained under standard laboratory conditions (12-h light/dark cycle, a constant temperature of 22 ± 2 °C, and 35%–55% humidity with food and water *ad libitum*). Mice aged 2–4 months were used in all experiments. After surgery, mice were housed individually for at least 1 week to allow for recovery prior to the experiments. We used only male mice for the behavioral tests and both male and female mice were randomly assigned to the other experimental groups. All experimental protocols were approved by the Xuzhou Medical University Institutional Animal Care and Use Committee (202110A238).

DBH-Cre (stock #T005671) and C57BL/6J mice were purchased from GemPharmatech. Primer *DBH-F*: GGGCAGTCTGGTACTTCCAAGCT and *DBH-R*: ACTGTGTCTTTGCACGAACGTG; *Actin-F*: CAGCAAAACC TGGCTGTGGATC and *Actin-R:* ATGAGCCACCATGTGGGTGTC were used for genotype identification.

Virus injection

All viruses used in this work were purchased from BrainVTA (China), except for the sparse labeling viruses (Brain Case, China). Briefly, mice (aged 8–12 weeks) were anesthetized with pentobarbital sodium (i. p. 90 mg/kg) and mounted on a stereotaxic frame (RWD, Shenzhen, China). The skull was exposed and craniotomies were performed. All virus injections were performed with a calibrated pulled-glass pipette (Sutter Instrument), and a microsyringe pump was used to control the injection volume and velocity (Stoelting Quintessential Injector). 0.1–0.3 µL of virus was injected at each site at a speed of 0.03 µL/min. After injection, the glass pipette was kept in place for an additional 10 min before being slowly withdrawn.

For anterograde labeling of the LC–aPC or LC–OB projections, rAAV-EF1α-DIO-EYFP was injected into the LC (AP, −5.5 mm; ML, ±0.8 mm; DV, −3.5 mm) of DBH-Cre mice. For retrograde labeling of the LC–aPC or LC–OB projections, AAV2/R-Ef1α-DIO-EYFP was injected into the OB (AP, +4.25 mm; ML, ±1.15 mm; DV, −1.9 mm) or aPC (AP, + 2.2 mm; ML, ±2.1 mm; DV, −4.6 mm) of DBH-Cre mice. To specifically infect OB-projecting LC NAergic neurons with eYFP and aPC-projecting LC NAergic neurons with mCherry, AAV2/R-Ef1α-DIO-EYFP and AAV2/R-Ef1α-DIO-mCherry were injected into the OB and aPC of DBH-Cre mice, respectively.

To specifically infect LC NAergic neurons with ChR2-eYFP, eYFP, hM4D-mCherry, or mCherry, rAAV2/9-EF1α-DIO-hChR2(134 R)-EYFP, rAAV-EF1α-DIO-EYFP, rAAV2/9-EF1α-DIO-hM4D-mCherry, or rAAV2/9-EF1α-DIO-mCherry was injected into LC of DBH-Cre mice. To selectively label a small number of NAergic neurons with eYFP, AAV-sparse-CSSP-eYFP-2E4 was into the LC of DBH-Cre mice.

To specifically infect OB and aPC-projecting LC neurons with hM4D-mCherry, hM3D-mCherry, or mCherry, rAAV2/R-hSyn-CRE-WPRE-hGH-pA was injected into the OB and aPC of C57BL/6J mice, and rAAV2/9-EF1α-DIO-hM4D-mCherry, rAAV2/9-EF1α-DIO-hM3D-mCherry or rAAV2/9-EF1α-DIO-mCherry was injected into the LC.

To specifically infect OB-projecting or aPC-projecting LC neurons with hM4D-mCherry or mCherry, rAAV2/R-hSyn-CRE-WPRE-hGH-pA was injected into OB or aPC of C57BL/6J mice, and rAAV2/9-EF1α-DIO-hM4D-mCherry or rAAV2/9-EF1α-DIO-mCherry was injected into the LC.

Optrode implantation

The optrode implantation procedure was similar to that our previously described[9,42,43]. Briefly, optrodes (op-tetrodes or op-microelectrodes) were implanted into the OB and the aPC to record spikes. Briefly, the mice were anesthetized with pentobarbital sodium (i.p. 90 mg/kg), mounted in a stereotaxic frame, and the fur on the surface of the scalp was removed. A hole was drilled above the left OB (AP, +4.0 mm; ML, +1.0) or aPC (AP, +2.15 mm; ML, +2.05 mm) for optrode (op-tetrode/op-microelectrode) implantation. Then, the optrode was implanted into the MCL of the OB lowered through the drilled hole to an average depth of 1.0–1.8 mm[43], or layer 2/3 of the aPC (DV, 4.0–4.5 mm). During the implantation, spikes were recorded to ensure optimal placement. A reference electrode was inserted into the skull and connected to the ground. Finally, the optrode was sealed to the bone and then a custom-made aluminum headplate was attached to the skull with dental acrylic. The signals recorded from the optrode were sent to a headstage and amplified by a 16-channel amplifier (Plexon DigiAmp; bandpass, 1–5000 Hz, 2000× gain), then sampled at 40 kHz by a Plexon Omniplex recording system. Mice were allowed to recover for at least 10 days after surgery before the start of recordings.

Immunohistochemistry

Mice were anaesthetized with pentobarbital sodium (i.p. 90 mg/kg), and perfused with room temperature saline, followed by ice-cold 4% phosphate-buffered paraformaldehyde. The brains were removed from the skull and post-fixed in 4% PFA for 8–10 h at 4 °C and subsequently dehydrated with 30% sucrose for 2–3 days at 4 °C. Brain tissues were embedded in OCT compound and cut in the coronal plane (20 µm) with a microtome (Leica CM1860). The sections were rinsed three times (10 min each time) with 0.01 M PBS and then blocked (10% normal goat serum, 0.25% Triton X-100 in PBS) for 90 min at room temperature, then subsequently incubated with primary antibodies (rabbit anti-TH; 1:200; Cat# AB152, Merck) diluted in blocking solution overnight at 4 °C. After washing three times in PBS, sections were incubated with a fluorescent secondary antibody (Alexa Fluor 488, Cat# A11034; Alexa Fluor 594, Cat# A11037; or Alexa Fluor 647, Cat# A32733; 1:500; Invitrogen) for 1.5 h at room temperature. Finally, the sections were washed in PBS and coverslipped with a mounting medium that included DAPI. Images were obtained with a confocal scanning microscope (Zeiss, LSM710).

3-D tissue imaging and image processing

Mice were anesthetized with pentobarbital sodium (i.p., 90 mg/kg), and perfused with room temperature saline, followed by ice-cold 4%

phosphate-buffered paraformaldehyde. Brains were dissected then incubated in 4% PFA at 4 °C with gentle shaking overnight and rinsed 3 times with 1×PBS for 2 h. Next, the fixed samples were cleared with Nuohai Enhanced Tissue Clearing Kit (NH-CR-230701, Nuohai Life Science, Shanghai). Briefly, brains were immersed in 30 ml of Solution A and gentle shaken at 4 °C for 7–8 days. The samples were rinsed 3 times with 1×PBS at room temperature and the PBS was refreshed every 2 h. Finally, 3-D fluorescence imaging of the cleared tissues was conducted with a Nuohai LS 18 tiling light sheet microscope (Nuohai Life Science, Shanghai; laser lines: 488 nm) and the images were processed in LS 18 ImageCombine software (Nuohai Life Science, Shanghai) and rendered in Amira (Thermo Fisher Scientific, USA).

Whole-cell recording

Mice were deeply anesthetized with pentobarbital sodium (i.p., 90 mg/kg) and quickly perfused with ice-cold oxygenated cutting solution (in mM, 85 NaCl, 2.5 KCl, 1.25 NaH_2PO_4, 25 $NaHCO_3$, 25 glucose, 75 sucrose, 0.5 $CaCl_2$, and 4 $MgCl_2$, equilibrated with 95% O_2 and 5% CO_2). The brain was quickly removed and placed in ice-cold oxygenated cutting solution. The OB (260 μm), aPC (260 μm), and LC (160 μm) were coronally sectioned using a vibratome (VT 1000S; Leica). The slices were recovered at 35 °C for 60 min in oxygenated artificial CSF (ACSF) containing (in mM): 119 NaCl, 2.5 KCl, 1.25 NaH_2PO_4, 2.5 $CaCl_2$, 1.3 $MgCl_2$, 1.3 $NaHCO_3$, and 10 glucose, equilibrated with 95% O_2 and 5% CO_2, and then the slices were allowed to recover at room temperature (25 °C) for 30 min before recordings. The slices were transferred to a recording chamber filled with ACSF (perfused at 2–3 ml/min) at room temperature for recording. The brain slices were visualized with an upright microscope equipped with a 60× water-immersion lens and an infrared-sensitive charge-coupled-device camera. Recording pipettes were pulled from borosilicate glass capillaries (P-1000, Sutter Instruments, USA).

To record action potentials (APs) and spontaneous excitatory postsynaptic currents (sEPSCs), the pipettes were filled with potassium-based internal solution (in mM: 135 K-gluconate, 5 KCl, 0.5 $CaCl_2$, 10 HEPES, 2 Mg-ATP, 0.1 GTP, and 5 EGTA, 290–300 mOsm, pH adjusted to 7.4 with KOH). APs were recorded in current/voltage-clamp mode and sEPSCs were recorded in voltage-clamp mode. To record current-evoked APs from aPC pyramidal neurons, eleven current steps (0, 20, 40, 60, 80, 100, 120, 140, 160, 180, and 200 pA; duration 400 ms) with a 30-s intertrial interval were applied. To isolate spontaneous excitatory postsynaptic currents (sEPSCs), $GABA_A$ receptors were blocked with bicuculline (10 μM, Tocris). The membrane potential was held at −65 mV.

To record spontaneous inhibitory postsynaptic currents (sIPSCs) in the OB, pipettes (5–8 MΩ) were filled with a cesium-based internal solution (in mM: 125 $CsMeSO_4$. 7 CsCl, 10 HEPES, 4 MgATP, 0.3 Na_3GTP, 0.5 EGTA, 10 Na_2- phosphocreatine, 5 QX-314, pH adjusted to 7.4 with CsOH, 290–300 mOsm) and the membrane potential was held at 0 mV. AMPA and NMDA receptors were blocked with 10 μM CNQX (Tocris), and 50 μM AP5 (Sigma), respectively.

To record spontaneous inhibitory postsynaptic currents (sIPSCs) in the aPC, the pipettes (5–8 MΩ) were filled with a cesium-based internal solution (in mM: 135 CsCl, 10 HEPES, 0.2 EGTA, 2 Na_2-ATP, 0.3 Na_3-GTP, and 10 glucose, pH adjusted to 7.4 with CsOH, 290–300 mOsm) and the membrane potential was held at −65 mV. AMPA receptors were blocked with 10 μM CNQX, and NMDA receptors were blocked with 50 μM AP5.

To examine the effect of NE on the activity of aPC pyramidal neurons, APs and postsynaptic currents were recorded via bath-applied NE (10 μM, MCE). To further examine the receptor types involved, NE (10 μM) was applied together with prazosin (2 μM, MCE), yohimbine (2 μM, MCE), or propranolol (2 μM, MCE).

To active LC $ChR2^+$ neurons, either constant blue light or blue light at different frequencies (473 nm; 10 ms pulses; 5, 10, 20 Hz) was delivered. To reveal the functional connection between LC NAergic neurons and the aPC/OB, spontaneous APs and postsynaptic currents (sEPSCs and sIPSCs) were recorded during optostimulation (473 nm; 10 ms-pulses; 10 Hz or 20 Hz for 1 min). An optogenetic system (Newdoon, Aurora-220) was used to generate the blue light (473 nm), which was delivered though an optical fiber placed near the recorded cell.

To silence LC hM4D-expressing neurons, CNO (BrainVTA) was applied after recording baseline spontaneous APs for 1 min (current-clamp mode).

All date were acquired via a MultiClamp 700B amplifier (Molecular Devices, San Jose, CA), filtered at 2 kHz, digitized with the Digidata 1440 A interface (Molecular Devices), and analyzed in Clampex 10.2 (Molecular Devices).

Odor presentation during in vivo electrophysiology recordings

The electrophysiology recordings procedure was consistent with that our previously described[42,56]. Briefly, six neutral odors (isoamyl acetate, 2-heptanone, benzaldehyde, n-heptane acid, n-pentanol, and 2-pentanone) from Sinopharm Chemical Reagent were dissolved in mineral oil at 1% (v/v) dilution and presented through an odor delivery system. During the period of odor delivery, a stream of nitrogen flowed through the oil before being diluted to 1/20 by an olfactometer. Odor presentation was controlled synchronously by the data acquisition system through a solenoid valve driven by a digital-to-analog converter. Air or odorized air was delivered in a randomized manner to the mouse's nose at a constant rate of 1 l/min to eliminate the effects of airflow. Each odor was presented for a total of 20 trials, with a duration of 2 s per trial and an intertrial interval of 12 s. This odor presentation paradigm was used only for passive odor stimulation. The animals did not exhibit selectivity towards any specific odors. We used a separate system for odor presentation in the go/no-go task (for details, see the "Go/no-go behavioral tasks" section, below).

In vivo electrophysiology recordings

Before recording the electrophysiology signals, mice were allowed to recover from surgery for at least 10 days. The head of the awake mouse was fixed with two horizontal bars, and the mouse was allowed to move freely on an air-supported free-floating Styrofoam ball. For spike recordings, the electrophysiology signals recorded from the optrode were sent to a headstage and then amplified by a 16-channel amplifier (Plexon DigiAmp; bandpass filtered at 300–5000 Hz, 2000× gain), then sampled at 40 kHz by a Plexon Omniplex recording system (1.17.1). Optostimulation (2-s trains delivered at 10 Hz and 20 Hz) was combined with odor presentation in a randomized manner. The electrophysiology signals and odor/light stimulation event markers were recorded by the Plexon Omniplex recording system. In the OB, although there are many types of cells, only the spikes from mitral or tufted cells are picked up by array/tetrode recording[57,58]. Mitral and tufted cells have large cell bodies, allowing their spikes to be recorded; other interneurons have small cell bodies and their spikes were not picked up or recorded. However, spikes from mitral and tufted cells could not be distinguished.

Behavioral tests

Go/no-go behavioral tasks. Mice were deprived of water for 48 h and maintained at 80%–85% of their initial weight during the entire experimental period. The experiment was divided into two parts: a go/go phase and a go/no-go phase that together lasted for 9 days. In the go/go phase (days 1 and 2), mice were trained to enter the odor port and lick on the water tube. The mice received a water reward when they licked the tube within a specific time window when either of two odors (0.01% isoamyl acetate or 0.01% 2-heptanone) was presented. In the go/no-go task (day 3 to day 9), the mice were trained to discriminate the two odors in order to receive the water reward. Odor discrimination

included an easy task and a difficult task. During the easy task (day 3 to day 5), the reinforced odor (S +) was isoamyl acetate (0.01%) and the unreinforced odor (S −) was 2-heptanone (0.01%). In the difficult task, the S+ was a 3:2 combination of isoamyl acetate (0.01%) and 2-heptanone (0.01%) and the S− was a 2:3 combination of isoamyl acetate (0.01%) and 2-heptanone (0.01%). Mice learned to lick a tube in the presence of the reinforced odor (S +) but not the unreinforced odor (S −). When an S+ odor was presented, the mice received the water reward for licking the tube (Hit) and did not receive a water reward if they did not lick (Miss). When the S− was present, the mice were punished with a 10-s refractory period if they licked the tube (false alarm: FA), and avoided punishment if they did not lick (correct rejection: CR). Hits and CRs were classed as correct responses, and Misses and FAs were classed as incorrect responses. Total accuracy was calculated as (number of Hits + number of CRs)/total number of trials. The Hit accuracy was calculated as (number of Hits/number of Misses + number of Hits). The CR accuracy was calculated as (number of CRs / number of CRs + number of FAs).

Buried pellet test

The buried pellet test was consistent with that our previously described[42,43]. Mice were deprived of food for 24 h prior to the test, but allowed to drink freely. On the first day of the buried pellet test, mice were habituated to the test cage (28-cm long, 17-cm wide and 13-cm high) for 5 min before the test. A food pellet (0.2 g) was buried 3-cm deep placed in a random corner of the test cage and the mouse was allowed to explore freely for 5 min. Performance was evaluated as the time taken to retrieve the food pellet. If the mouse failed to find the food pellet, the time was recorded as 5 min. On the second day, the visible pellet test was performed, which was similar to the buried pellet test except that the food pellet was placed on top of the bedding.

Olfactory preference/avoidance tests

The olfactory preference/avoidance tests were consistent with that our previously described[42,43]. A custom-designed test cage (45-cm long, 35-cm wide and 25-cm high) with two equal chambers was used to assess olfactory preference/avoidance behavior. Peanut butter and TMT were used the attractant and aversive odorants, respectively. Before the test, the mice were placed into the chamber and allowed to freely explore for 10 min. Then a cotton swab containing an odorant (peanut butter or TMT) was placed in one compartment and a swab containing the mineral oil was placed in the other compartment. The time spent in each chamber was measured for 10 min. The RTPP index was calculated as (time in the odorant side − time in the mineral oil side)/(time in the odorant side + time in the mineral oil side). Behavior was recorded by an infrared camera and the videos were analyzed in EthoVision XT 15.

Open-field test

Mice were individually introduced to an open-field chamber (50-cm long, 50-cm wide, and 40-cm high) and allowed to explore for 10 min. The central area was defined as a central square covering 50% of the OFT area. Movement paths were recorded by a video camera and analyzed in EthoVision XT 15. The total distance traveled was used to evaluate locomotor activity, and the distance in the central area was used to evaluate anxiety-like behavior.

Chemogenetic manipulation

The designer drug CNO (i.p., 3 mg/kg) was administrated 30–40 min before the start of experiments, including the go/no-go behavioral tasks, the buried pellet test, the olfactory preference/avoidance tests and the open-field test.

Quantification and statistical analyses

Quantification of immunostaining of NAergic neurons. To quantify the number of NAergic neurons projecting to the aPC and OB, the LC was coronally sectioned (20 μm) and non-consecutive sections were randomly collected for TH immunostaining. Images were taken from regions of the LC on a confocal scanning microscope with a 20× objective (Zeiss, LSM710), then processed in ZEN 2011 (Zeiss). The number of eYFP-, mCherry-, TH-, eYFP/TH-, mCherry/TH-, and eYFP/mCherry/TH-positive nuclei per area was calculated for the total LC region. Quantification of co-localization was performed in ZEN 3.4. The number of sections and brains used for the co-localization analysis are provided in the figure legends. All schematics were created using Adobe Illustrator software.

Statistics of the in vitro electrophysiological data

To test whether light evoked a significant response, the spontaneous firing rate of aPC pyramidal neurons was calculated by averaging the spikes before (baseline, 0–60 s) and during (60–120 s) optostimulation within 2-s bins. In the OB mitral cells, we used two computational methods simultaneously. Firstly, the spontaneous firing rate of mitral cells was calculated by averaging the spikes before optostimulation (baseline, 0–60 s) and during (60–120 s) optostimulation within 2-s bins to screen for excitatory responses. Next, the spontaneous firing rate of mitral cells was calculated by averaging the spikes before optostimulation (baseline, 0–60 s) and 40 s after the start of optostimulation until 40 s after the end of optostimulation (100–160 s) within 2-s bins to screen for inhibitory responses. To examine whether a response during optostimulation were significant, we used a two-sided paired t-test to compare the baseline spiking with spiking during optostimulation. $p > 0.05$ was defined as nonresponsive and $p < 0.05$ was defined as responsive. All responsive cells were further categorized as being excitatory or inhibitory responses.

Off-line spike sorting and statistics of the unit data

Spikes were sorted from the raw data with Offline Sorter V4 software (Plexon). The separation of different units was performed by principal component analysis. A unit was classified as a single unit if <0.75% of the inter spike-intervals were <1 ms. This resulted in unimodal firing-rate distributions. The data 2 s before and 4 s after the onset of each odor stimulation event were extracted and a peristimulus time histogram (PSTH) was generated by averaging the spike firing rate within 100 ms bins. The spontaneous firing rate was calculated by averaging across the spikes fired during the 2 s before odor stimulation (baseline); the odor-evoked firing rate was calculated by averaging across the spikes fired during the 2 s after the onset of odor stimulation. To avoid contamination by potential multi-units, units with a spontaneous firing rate higher than 25 Hz were excluded from further analysis. The cluster quality was quantified using L-ratio and isolation distance (Supplementary Table. 1). To test whether an odor evoked a significant response, we used a two-sided paired t-test to compare the baseline firing rate with the odor-evoked firing rate across all the trials for each cell–odor pair. If $p > 0.05$, the unit–odor pair was defined as non-responsive. If $p < 0.05$, the unit–odor pair was defined as responsive and was further categorized as excitatory or inhibitory.

Odor decoding analysis

The odor decoding analysis was based on population activity and was conducted in Python 3.7.4 by a support vector machine (SVM) algorithm with a linear kernel. Decoding was conducted on trial data pooled across all recording sessions. Input to the algorithm consisted of activity vectors derived from single-trial responses, where the length of the vector was determined by the number of neurons times the number of time bins (bin size = 100 ms). The classification was based on concatenated bins, where activity vectors were obtained from a series of non-overlapping time bins (e.g., for t = 500 ms, the input consisted of five bins evenly divided over the 0–500 ms after odor stimulation). Ten-fold cross-validation was used to divide the training set and test set and then compute classification accuracy.

Accuracy was defined as the fraction of test trials that were correctly identified. As a control, the classification accuracy during the 2-s period before odor onset was assessed via the same method.

Statistical analyses

All Data are presented as means ± SEM. Statistical comparisons were performed in GraphPad Prism 9.0 or MATLAB2020b. All behavioral and in vivo electrophysiological data collection were randomized and investigators were blinded to experimental conditions during the analyses. Normally distributed data were tested by two-sided paired / unpaired t-tests or one-way/two-way ANOVA followed by post hoc Dunnett's test or Tukey's test for multiple comparisons. Non-normally distributed data were analyzed by a Wilcoxon rank sum test, Wilcoxon matched-pairs signed rank test, or Kruskal-Wallis test. Significance levels are indicated by $^{*}p < 0.05$, $^{**}p < 0.01$, $^{***}p < 0.001$, $^{****}p < 0.0001$.

Reporting summary

Further information on research design is available in the Nature Portfolio Reporting Summary linked to this article.

Data availability

Source data are provided as a Source Data file at https://codeocean.com/capsule/7909289/tree. Further information regarding to the findings in this study are available from the corresponding authors. Source data are provided with this paper.

Code availability

All codes can be found at Code Ocean through the link: https://codeocean.com/capsule/7909289/tree.

References

1. Uchida, N., Poo, C. & Haddad, R. Coding and transformations in the olfactory system. *Annu. Rev. Neurosci.* **37**, 363–385 (2014).
2. Li, A., Rao, X., Zhou, Y. & Restrepo, D. Complex neural representation of odour information in the olfactory bulb. *Acta Physiol.* **228**, e13333 (2020).
3. Vaaga, C. E. & Westbrook, G. L. Parallel processing of afferent olfactory sensory information. *J. Physiol.* **594**, 6715–6732 (2016).
4. Imai, T. Construction of functional neuronal circuitry in the olfactory bulb. *Semin. Cell Dev. Biol.* **35**, 180–188 (2014).
5. Imamura, F., Ito, A. & LaFever, B. J. Subpopulations of projection neurons in the olfactory bulb. *Front. Neural Circuits* **14**, 561822 (2020).
6. Davison, I. G. & Ehlers, M. D. Neural circuit mechanisms for pattern detection and feature combination in olfactory cortex. *Neuron* **70**, 82–94 (2011).
7. Bolding, K. A. & Franks, K. M. Complementary codes for odor identity and intensity in olfactory cortex. *Elife* **6**, e22630 (2017).
8. Roland, B., Deneux, T., Franks, K. M., Bathellier, B. & Fleischmann, A. Odor identity coding by distributed ensembles of neurons in the mouse olfactory cortex. *Elife* **6**, e26337 (2017).
9. Wang, D. et al. Task-demand-dependent neural representation of odor information in the olfactory bulb and posterior piriform cortex. *J. Neurosci.* **39**, 10002–10018 (2019).
10. Li, A., Gire, D. H. & Restrepo, D. Upsilon spike-field coherence in a population of olfactory bulb neurons differentiates between odors irrespective of associated outcome. *J. Neurosci.* **35**, 5808–5822 (2015).
11. Wang, D. et al. Serotonergic afferents from the dorsal raphe decrease the excitability of pyramidal neurons in the anterior piriform cortex. *Proc. Natl Acad. Sci. USA* **117**, 3239–3247 (2020).
12. Steinfeld, R., Herb, J. T., Sprengel, R., Schaefer, A. T. & Fukunaga, I. Divergent innervation of the olfactory bulb by distinct raphe nuclei. *J. Comp. Neurol.* **523**, 805–813 (2015).
13. Lottem, E., Lorincz, M. L. & Mainen, Z. F. Optogenetic activation of dorsal raphe serotonin neurons rapidly inhibits spontaneous but not odor-evoked activity in olfactory cortex. *J. Neurosci.* **36**, 7–18 (2016).
14. Zhou, P., Liu, P., Zhang, Y., Wang, D. & Li, A. The response dynamics and function of cholinergic and GABAergic neurons in the basal forebrain during olfactory learning. *Front. Cell Neurosci.* **16**, 911439 (2022).
15. Zaborszky, L., Carlsen, J., Brashear, H. R. & Heimer, L. Cholinergic and GABAergic afferents to the olfactory bulb in the rat with special emphasis on the projection neurons in the nucleus of the horizontal limb of the diagonal band. *J. Comp. Neurol.* **243**, 488–509 (1986).
16. Wen, P. et al. Cortical organization of centrifugal afferents to the olfactory bulb: mono- and trans-synaptic tracing with recombinant neurotropic viral tracers. *Neurosci. Bull.* **35**, 709–723 (2019).
17. Patil, M. M., Linster, C., Lubenov, E. & Hasselmo, M. E. Cholinergic agonist carbachol enables associative long-term potentiation in piriform cortex slices. *J. Neurophysiol.* **80**, 2467–2474 (1998).
18. Schwarz, L. A. & Luo, L. Organization of the locus coeruleus-norepinephrine system. *Curr. Biol.* **25**, R1051–R1056 (2015).
19. Sara, S. J. The locus coeruleus and noradrenergic modulation of cognition. *Nat. Rev. Neurosci.* **10**, 211–223 (2009).
20. Horie, S. et al. Structural basis for noradrenergic regulation of neural circuits in the mouse olfactory bulb. *J. Comp. Neurol.* **529**, 2189–2208 (2021).
21. Datiche, F. & Cattarelli, M. Catecholamine innervation of the piriform cortex: a tracing and immunohistochemical study in the rat. *Brain Res.* **710**, 69–78 (1996).
22. Liang, Y. et al. The NAergic locus coeruleus-ventrolateral preoptic area neural circuit mediates rapid arousal from sleep. *Curr. Biol.* **31**, 3729–3742.e3725 (2021).
23. Uematsu, A., Tan, B. Z. & Johansen, J. P. Projection specificity in heterogeneous locus coeruleus cell populations: implications for learning and memory. *Learn Mem.* **22**, 444–451 (2015).
24. Chowdhury, A. et al. A locus coeruleus-dorsal CA1 dopaminergic circuit modulates memory linking. *Neuron* **110**, 3374–3388.e3378 (2022).
25. Doucette, W., Milder, J. & Restrepo, D. Adrenergic modulation of olfactory bulb circuitry affects odor discrimination. *Learn Mem.* **14**, 539–547 (2007).
26. Rangel, S. & Leon, M. Early odor preference training increases olfactory bulb norepinephrine. *Brain Res. Dev. Brain Res.* **85**, 187–191 (1995).
27. Ghosh, A. et al. Locus coeruleus activation patterns differentially modulate odor discrimination learning and odor valence in rats. *Cereb. Cortex Commun.* **2**, tgab026 (2021).
28. Linster, C. et al. Noradrenergic activity in the olfactory bulb is a key element for the stability of olfactory memory. *J. Neurosci.* **40**, 9260–9271 (2020).
29. de Almeida, L., Reiner, S. J., Ennis, M. & Linster, C. Computational modeling suggests distinct, location-specific function of norepinephrine in olfactory bulb and piriform cortex. *Front. Comput. Neurosci.* **9**, 73 (2015).
30. Schwarz, L. A. et al. Viral-genetic tracing of the input-output organization of a central noradrenaline circuit. *Nature* **524**, 88–92 (2015).
31. McLean, J. H., Shipley, M. T., Nickell, W. T., Aston-Jones, G. & Reyher, C. K. Chemoanatomical organization of the noradrenergic input from locus coeruleus to the olfactory bulb of the adult rat. *J. Comp. Neurol.* **285**, 339–349 (1989).
32. Devore, S. & Linster, C. Noradrenergic and cholinergic modulation of olfactory bulb sensory processing. *Front. Behav. Neurosci.* **6**, 52 (2012).
33. Linster, C., Nai, Q. & Ennis, M. Nonlinear effects of noradrenergic modulation of olfactory bulb function in adult rodents. *J. Neurophysiol.* **105**, 1432–1443 (2011).

34. Shipley, M. T. & Ennis, M. Functional organization of olfactory system. *J. Neurobiol.* **30**, 123–176 (1996).
35. Bouret, S. & Sara, S. J. Locus coeruleus activation modulates firing rate and temporal organization of odour-induced single-cell responses in rat piriform cortex. *Eur. J. Neurosci.* **16**, 2371–2382 (2002).
36. Shea, S. D., Katz, L. C. & Mooney, R. Noradrenergic induction of odor-specific neural habituation and olfactory memories. *J. Neurosci.* **28**, 10711–10719 (2008).
37. Ghosh, A., Purchase, N. C., Chen, X. & Yuan, Q. Norepinephrine modulates pyramidal cell synaptic properties in the anterior piriform cortex of mice: age-dependent effects of beta-adrenoceptors. *Front. Cell Neurosci.* **9**, 450 (2015).
38. Nai, Q., Dong, H. W., Hayar, A., Linster, C. & Ennis, M. Noradrenergic regulation of GABAergic inhibition of main olfactory bulb mitral cells varies as a function of concentration and receptor subtype. *J. Neurophysiol.* **101**, 2472–2484 (2009).
39. Mandairon, N. et al. Noradrenergic modulation in the olfactory bulb influences spontaneous and reward-motivated discrimination, but not the formation of habituation memory. *Eur. J. Neurosci.* **27**, 1210–1219 (2008).
40. Escanilla, O., Arrellanos, A., Karnow, A., Ennis, M. & Linster, C. Noradrenergic modulation of behavioral odor detection and discrimination thresholds in the olfactory bulb. *Eur. J. Neurosci.* **32**, 458–468 (2010).
41. Steindler, D. A. Locus coeruleus neurons have axons that branch to the forebrain and cerebellum. *Brain Res.* **223**, 367–373 (1981).
42. Wang, D. et al. VIP interneurons regulate olfactory bulb output and contribute to odor detection and discrimination. *Cell Rep.* **38**, 110383 (2022).
43. Chen, F. et al. alpha-Synuclein aggregation in the olfactory bulb induces olfactory deficits by perturbing granule cells and granular-mitral synaptic transmission. *NPJ Parkinsons Dis.* **7**, 114 (2021).
44. Suzuki, N. & Bekkers, J. M. Inhibitory interneurons in the piriform cortex. *Clin. Exp. Pharmacol. Physiol.* **34**, 1064–1069 (2007).
45. Nagayama, S., Homma, R. & Imamura, F. Neuronal organization of olfactory bulb circuits. *Front. Neural Circuits* **8**, 98 (2014).
46. Batista-Brito, R., Close, J., Machold, R. & Fishell, G. The distinct temporal origins of olfactory bulb interneuron subtypes. *J. Neurosci.* **28**, 3966–3975 (2008).
47. Zhao, P. et al. Upper brainstem cholinergic neurons project to ascending and descending circuits. *BMC Biol.* **21**, 135 (2023).
48. McBurney-Lin, J., Lu, J., Zuo, Y. & Yang, H. Locus coeruleus-norepinephrine modulation of sensory processing and perception: a focused review. *Neurosci. Biobehav. Rev.* **105**, 190–199 (2019).
49. Nai, Q., Dong, H. W., Linster, C. & Ennis, M. Activation of alpha1 and alpha2 noradrenergic receptors exert opposing effects on excitability of main olfactory bulb granule cells. *Neuroscience* **169**, 882–892 (2010).
50. Hayar, A., Heyward, P. M., Heinbockel, T., Shipley, M. T. & Ennis, M. Direct excitation of mitral cells via activation of alpha1-noradrenergic receptors in rat olfactory bulb slices. *J. Neurophysiol.* **86**, 2173–2182 (2001).
51. Jin, X. et al. Identification of a Group of GABAergic neurons in the dorsomedial area of the locus coeruleus. *PLoS ONE* **11**, e0146470 (2016).
52. Breton-Provencher, V. & Sur, M. Active control of arousal by a locus coeruleus GABAergic circuit. *Nat. Neurosci.* **22**, 218–228 (2019).
53. Guerin, D., Peace, S. T., Didier, A., Linster, C. & Cleland, T. A. Noradrenergic neuromodulation in the olfactory bulb modulates odor habituation and spontaneous discrimination. *Behav. Neurosci.* **122**, 816–826 (2008).
54. Benarroch, E. E. Locus coeruleus. *Cell Tissue Res.* **373**, 221–232 (2018).
55. Li, L. et al. Stress accelerates defensive responses to looming in mice and involves a locus coeruleus-superior colliculus projection. *Curr. Biol.* **28**, 859–871 e855 (2018).
56. Wu, T. et al. Olfactory-auditory sensory integration in the lateral entorhinal cortex. *Prog. Neurobiol.* **221**, 102399 (2023).
57. Kay, L. M. & Laurent, G. Odor- and context-dependent modulation of mitral cell activity in behaving rats. *Nat. Neurosci.* **2**, 1003–1009 (1999).
58. Doucette, W. et al. Associative cortex features in the first olfactory brain relay station. *Neuron* **69**, 1176–1187 (2011).

Acknowledgements

This work was supported by the Key Technologies Research and Development Program (2021ZD0203100), the National Natural Science Foundation of China (NSFC, 32271055 and 32070995 to A.L.), and the Jiangsu Province Innovative and Entrepreneurial Team Program to H.Z. and A.L.

Author contributions

C.G., R.L., H.Z., and A.L. designed the research; C.G., R.L., Y.P., Z.W., and C.L. performed the research; C.G., S.L., and P.L. analyzed the data; C.G. and A.L. wrote the paper.

Competing interests

The authors declare no competing interests.

Additional information

Supplementary information The online version contains supplementary material available at https://doi.org/10.1038/s41467-024-55609-9.

Correspondence and requests for materials should be addressed to Anan Li.

Peer review information *Nature Communications* thanks Kazunori Toida, and the other, anonymous, reviewer(s) for their contribution to the peer review of this work. A peer review file is available.